AD-A161 720 ULTRASONIC MODEL INVESTIGATION OF THE EFFECTS OF LATERAL HETEROGENEITIES O (U) AMERICAN CHEMICAL SOCIETY SPRINGFIELD VA DIV OF INDUSTRIAL AN M N TOKSOEZ 1/1

UNCLASSIFIED 10 SEP 85 ARO-18022 3-GS DAAG29-81-K-0145 F/G 8/11 NL

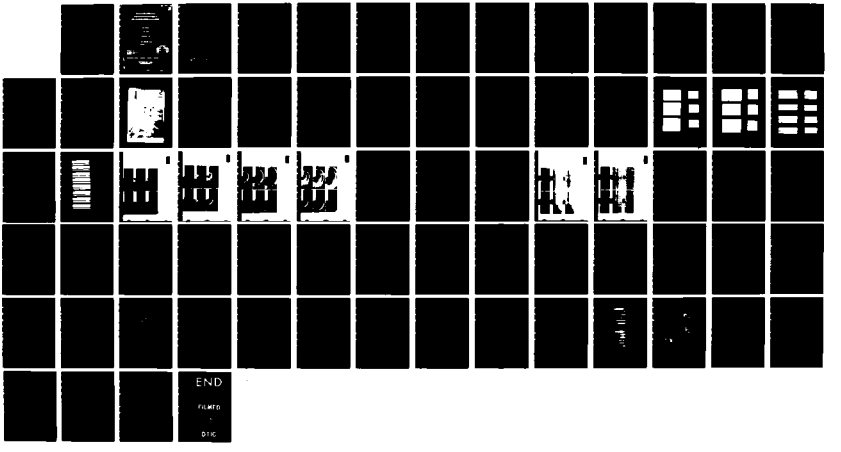

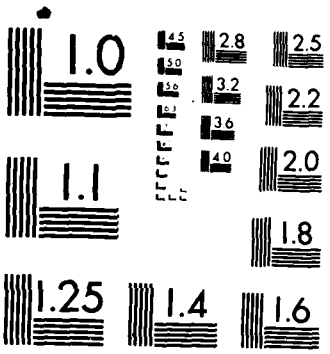

AD-A161 720

DTIC FILE COPY

Earth Resources Laboratory

Massachusetts Institute of Technology, 42 Carleton St., Cambridge, MA 02142

Original contains color plates: All DTIC reproductions will be in black and white

DTIC ELECTE DEC 12 1985 S D

88 11 18 255

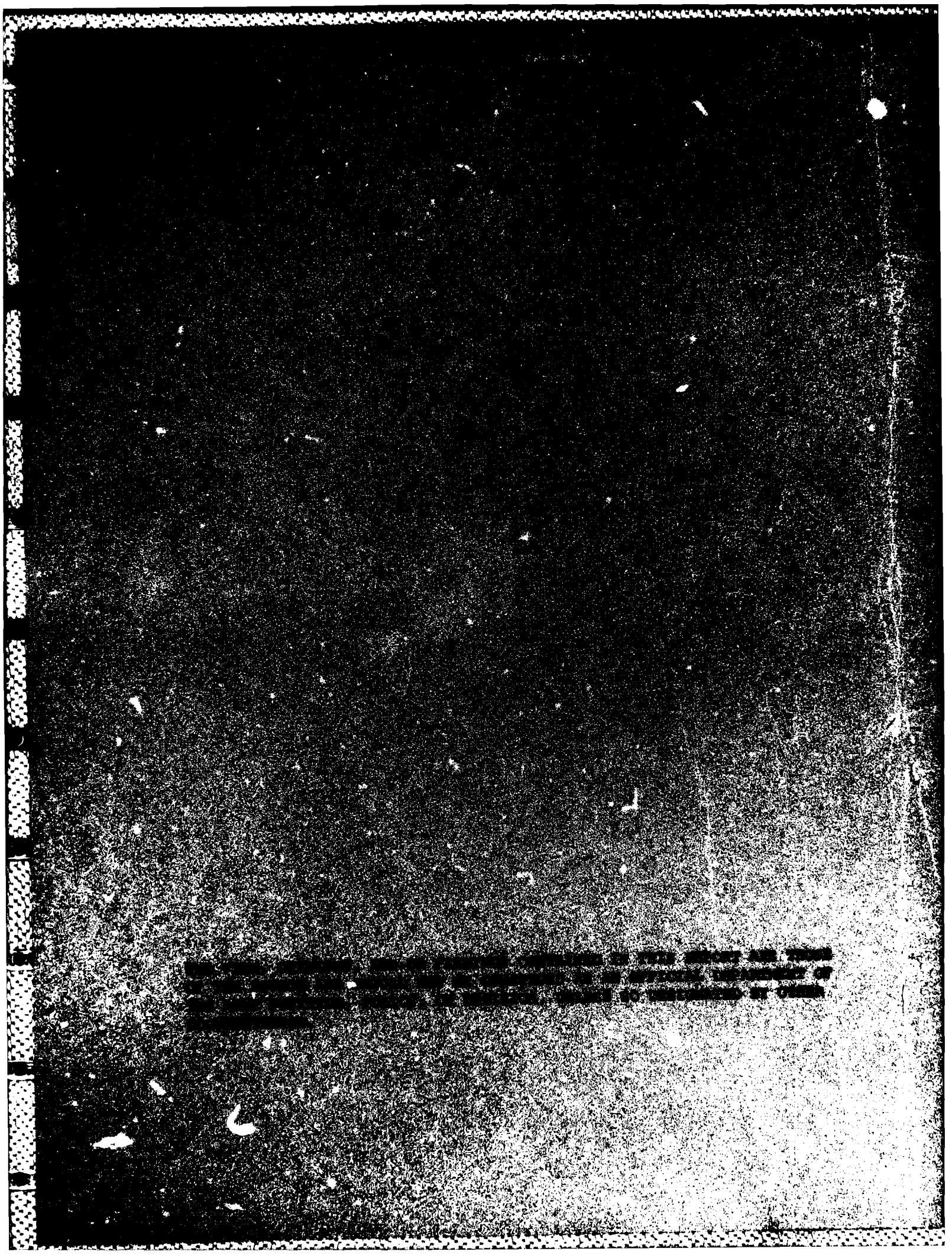

UNCLASSIFIED
SECURITY CLASSIFICATION OF THIS PAGE (When Data Entered)

REPORT DOCUMENTATION PAGE

READ INSTRUCTIONS BEFORE COMPLETING FORM

1. REPORT NUMBER: ARO 18022.3-GS	2. GOVT ACCESSION NO.: N/A
3. RECIPIENT'S CATALOG NUMBER: N/A	
4. TITLE (and Subtitle): Ultrasonic model investigations of the effects of lateral heterogeneities on seismic surface wave propagation and scattering	5. TYPE OF REPORT & PERIOD COVERED: Final 8/1/81-5/31/84
	6. PERFORMING ORG. REPORT NUMBER
7. AUTHOR(s): M. Nafi Toksöz	8. CONTRACT OR GRANT NUMBER(s): DAAG29-81-K-0145
9. PERFORMING ORGANIZATION NAME AND ADDRESS: Earth Resources Laboratory, Department of Earth, Atmospheric, and Planetary Sciences, Massachusetts Institute of Technology, Cambridge, MA 02139	10. PROGRAM ELEMENT, PROJECT, TASK AREA & WORK UNIT NUMBERS
11. CONTROLLING OFFICE NAME AND ADDRESS: U. S. Army Research Office, Post Office Box 12211, Research Triangle Park, NC 27709	12. REPORT DATE: 10 September 1985
	13. NUMBER OF PAGES
14. MONITORING AGENCY NAME & ADDRESS (if different from Controlling Office)	15. SECURITY CLASS. (of this report): Unclassified
	15a. DECLASSIFICATION/DOWNGRADING SCHEDULE

16. DISTRIBUTION STATEMENT (of this Report)

Approved for public release; distribution unlimited.

17. DISTRIBUTION STATEMENT (of the abstract entered in Block 20, if different from Report)

NA

18. SUPPLEMENTARY NOTES

The view, opinions, and/or findings contained in this report are those of the author(s) and should not be construed as an official Department of the Army position, policy, or decision, unless so designated by other documentation.

19. KEY WORDS (Continue on reverse side if necessary and identify by block number)

Ultrasonic Modelling, Rayleigh Waves, Scattering, Attenuation, Tibet

20. ABSTRACT (Continue on reverse side if necessary and identify by block number)

The effects of topographic features on Rayleigh wave propagation and scattering are investigated using two and three-dimensional ultrasonic models. Starting from simple steps, different topographic features are modeled. The effects of these features on Rayleigh wave transmission and scattering are examined as a function of wavelength. In general, backscattered or reflected Rayleigh waves are small compared to transmitted waves. A significant fraction of the Rayleigh wave energy is scattered into body waves. To complement the laboratory studies, two-dimensional finite difference calculations are

DD FORM 1 JAN 73 1473 EDITION OF 1 NOV 65 IS OBSOLETE

UNCLASSIFIED
SECURITY CLASSIFICATION OF THIS PAGE (When Data Entered)

carried out. These show the details of the scattering of incident Rayleigh waves at a step discontinuity into P, S and Rayleigh waves. More energy scatters into S waves than into P waves.

Using three-dimensional laboratory models of steps, the dependence of wave scattering on angle of incidence is studied. Transmission and reflection coefficients (transmitted or reflected energy/incident energy) computed from spectral ratios vary strongly with incidence angle. At wavelengths equal to twice the step height, the fraction of incident energy scattered into body waves ranges from more than 90% at normal incidence to about zero at near-grazing incidence. At each angle, transmission coefficients vary strongly with frequency. Because of frequency-dependent phase shifts, the transmitted and reflected waves are distorted.

The effect of the steps on the propagation of Rayleigh waves is demonstrated by convolving synthetic dispersed wave trains with the impulse response of the scale models. The ocean-continent margin of the western United States is modeled as a 60° ramp scaled to 60 km height. The Tibetan Plateau is modeled as a broad mesa scaled to 40 km height. In both models the azimuthal dependence of transmitted Rayleigh waves is similar to that observed at WWSSN stations for Rayleigh waves crossing the modeled terrestrial structures.

ULTRASONIC MODEL INVESTIGATION OF THE EFFECTS OF LATERAL HETEROGENEITIES ON SEISMIC SURFACE WAVE PROPAGATION AND SCATTERING

FINAL REPORT

M. NAFI TOKSÖZ

10 September 1985

U.S. ARMY RESEARCH OFFICE

DAAG29-81-K-0145

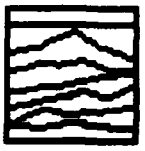

Earth
Resources
Laboratory

Massachusetts Institute of Technology, 42 Carleton St., Cambridge, MA 02142

APPROVED FOR PUBLIC RELEASE;
DISTRIBUTION UNLIMITED.

ABSTRACT

The effects of topographic features on Rayleigh wave propagation and scattering are investigated in the laboratory using three-dimensional ultrasonic models. Starting from simple steps, different topographic features are modeled. The effects of these features on Rayleigh wave transmission and scattering are examined as a function of wavelength and as a function of angle of incidence. In general, backscattered or reflected Rayleigh waves are small compared to transmitted waves. A significant fraction of the Rayleigh wave energy is scattered into body waves. To complement the laboratory studies, two-dimensional finite difference calculations are carried out. These show the details of the scattering of incident Rayleigh waves at a step discontinuity into P, S, and Rayleigh waves. More energy scatters into S waves than into P waves.

Using three-dimensional laboratory models of steps, the dependence of wave scattering on angle of incidence is studied. Transmission and reflection coefficients (transmitted or reflected energy/incident energy) computed from spectral ratios vary strongly with incidence angle. At wavelengths equal to twice the step height, the fraction of incident energy scattered into body waves ranges from more than 90% at normal incidence to about zero at near-grazing incidence. At each angle, transmission coefficients vary strongly with frequency. Because of frequency-dependent phase shifts, the transmitted and reflected waves are distorted.

The effect of the steps on the propagation of Rayleigh waves is demonstrated by convolving synthetic dispersed wave trains with the impulse response of the scale models. The ocean-continent margin of the western United States is modeled as a 60° ramp scaled to 60 km height. The Tibetan Plateau is modeled as a broad mesa scaled to 40 km height. In both models the azimuthal dependence of transmitted Rayleigh waves is similar to that observed

at WWSSN stations for Rayleigh waves crossing the modeled terrestrial structures.

TABLE OF CONTENTS

I. INTRODUCTION

Lateral crustal heterogeneities have an important influence on the propagation of surface waves. In Figure 1, long-period surface waves recorded from an isotropic source (m_b = 7 explosion) in Eastern Kazakhstan are shown at Eurasian stations. Surface waves crossing Tibet and the Himalayas are severely attenuated. These observations are similar to those of Bird and Toksöz (1977). Similarly, Rayleigh waves recorded from a nuclear explosion at the Nevada Test Site are strongly attenuated as they cross the Pacific margin as shown in Figure 2. In recent years studies have concentrated on regional variations of the lithosphere and mantle structures. The effects of such heterogeneities on surface waves have been considered primarily in terms of deviation of propagation paths from the "great circle" path and multipathing effects (Yomogida and Aki, 1985). Yet as Figures 1 and 2 show, major topographic features and sharp structural contrasts at ocean-continent boundaries, active subduction zones and continental collision belts could have significant effects on surface wave amplitude attenuation due to scattering.

Higher modes of surface waves are affected by propagation across lateral heterogeneities as well. Rusaikin *et al.* (1977) showed that *Lg* was absent from paths crossing Tibet, and proposed three possible explanations for this absence: (1) abrupt changes in crustal structure at the plateau margins, (2) unusual velocity structure beneath the plateau, and (3) low-Q regions within the plateau. Chinn *et al.* (1980) studied the propagation of *Lg* in the Andes, and suggested that the primary factor in the efficient propagation of *Lg* is the orientation of the path relative to the structural trend of the mountains: efficient *Lg* propagation parallel to the structural trend, inefficient propagation perpendicular to that trend. Baumgardt (1985) found a similar behavior for propagation across the Urals. The purpose of our study is to understand the surface wave scattering across topographical and structural heterogeneities

using ultrasonic modeling. In ultrasonic laboratory studies we observe exactly the same trend of waves attenuating strongly across structural heterogeneities. Figure 3 shows laboratory results of Rayleigh wave propagation in a model of Nevada Basin and Range structure. Note that from a point source at S, the Rayleigh wave propagating parallel to the structural trend (R_1) is much larger than those that go across the trend (R_2 and R_3). In the direction parallel to the trend, the wave shows relatively little scattering, while normal to the trend wave shapes have been altered and attenuated because of strong scattering. These effects are investigated in detail in the next sections using both two- and three-dimensional models.

REFERENCES

Baumgardt, D.R., 1985. Scattering attenuation of P and Lg waves and P-coda and Lg yield estimation. Paper presented at 7th Ann. DARPA/AFGL Seismic Research Symp.

Bird, P. and M.N. Toksöz, 1977. Strong attenuation of Rayleigh waves in Tibet, *Nature*, *266*, 161-163.

Chinn, D.S., B.L. Isacks and M. Barazangi, 1980. High-frequency seismic wave propagation in Western South America along the continental margin, in the Nazca plate and across the Altiplano, *Geophys. Jour. R. Astro. Soc.*, *60*, (2), 209-244.

McGarr, A., 1969. Amplitude variations of Rayleigh waves - propagation across a continental margin, *Bull. Seis. Soc. Am.*, *59*, 1281-1305.

Rusaikin, A., I. Nersesov, V. Khalturin and P. Molnar, 1977. Propagation of Lg and lateral variations in crustal structure in Asia, *Jour. Geophys. Res.*, *82*, 307-316.

Yomogida, K. and K. Aki, 1985. Waveform synthesis of surface waves in a laterally heterogeneous earth by the Gaussian beam method, *Jour. Geophys. Res.*, *90*, 7665-7688.

FIGURE CAPTIONS

Figure 1. Long period vertical component surface waves recorded at WWSSN stations (triangles) from M_b = 7 explosion of 11/30/69 (Eastern Kazakhstan).

Figure 2. Rayleigh waves crossing the continent-ocean boundary; seismograms from the nuclear explosion Boxcar, recorded at Berkeley (BRK) and Ocean Bottom Seismometer (OBS) in the Pacific. At top locations of the Nevada Test Site, BRK and OBS stations and the path are shown. Traces (a) and (b) are raw (unnormalized) seismograms at BRK and OBS, respectively. The two traces at (c) are filtered and gain-normalized. The solid trace is BRK and the dashed trace OBS. Note that amplitude decreases by about a factor of 3 when the wave crosses the continent-ocean margin (after McGarr, 1969).

Figure 3. Data taken with valleys filled with two parallel layers. Effects of topography and layered valley on Rayleigh wave scattering and dispersion. Model of Dry Lake Valley, Nevada (scale 1:250,000).

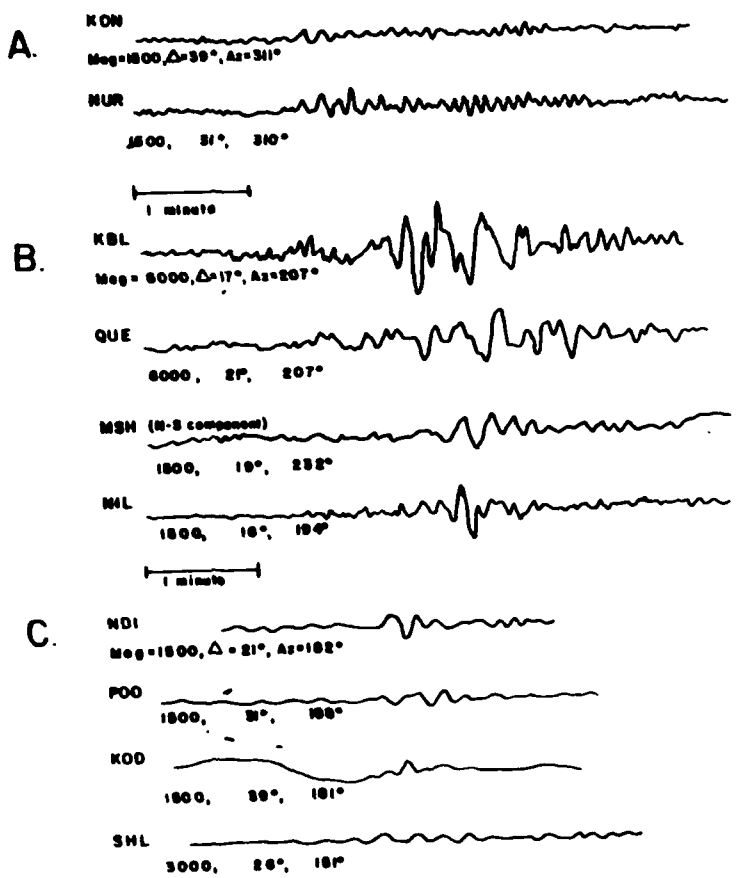
A.
KON
Mag=1800, Δ=39°, Az=311°
NUR
1800, 31°, 310°
1 minute
B.
KBL
Mag = 6000, Δ=17°, Az=207°
QUE
6000, 21°, 207°
MSH (N-S component)
1800, 19°, 252°
NIL
1800, 19°, 194°
1 minute
C.
NDI
Mag=1800, Δ = 21°, Az=182°
POO
1800, 31°, 188°
KOD
1800, 38°, 181°
SHL
3000, 26°, 181°

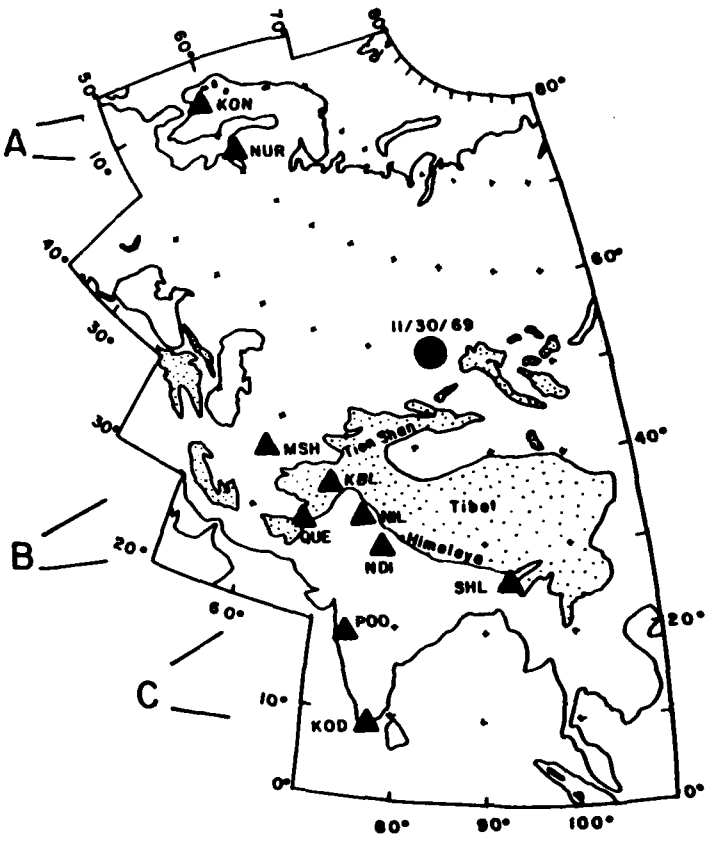
A
B
C
KON
NUR
MSH
KBL
QUE
NIL
NDI
POO
KOD
SHL
11/30/69
Tien Shan
Tibet
Himalaya
60°
80°
40°
30°
20°
10°
0°
90°
100°

Figure 1.

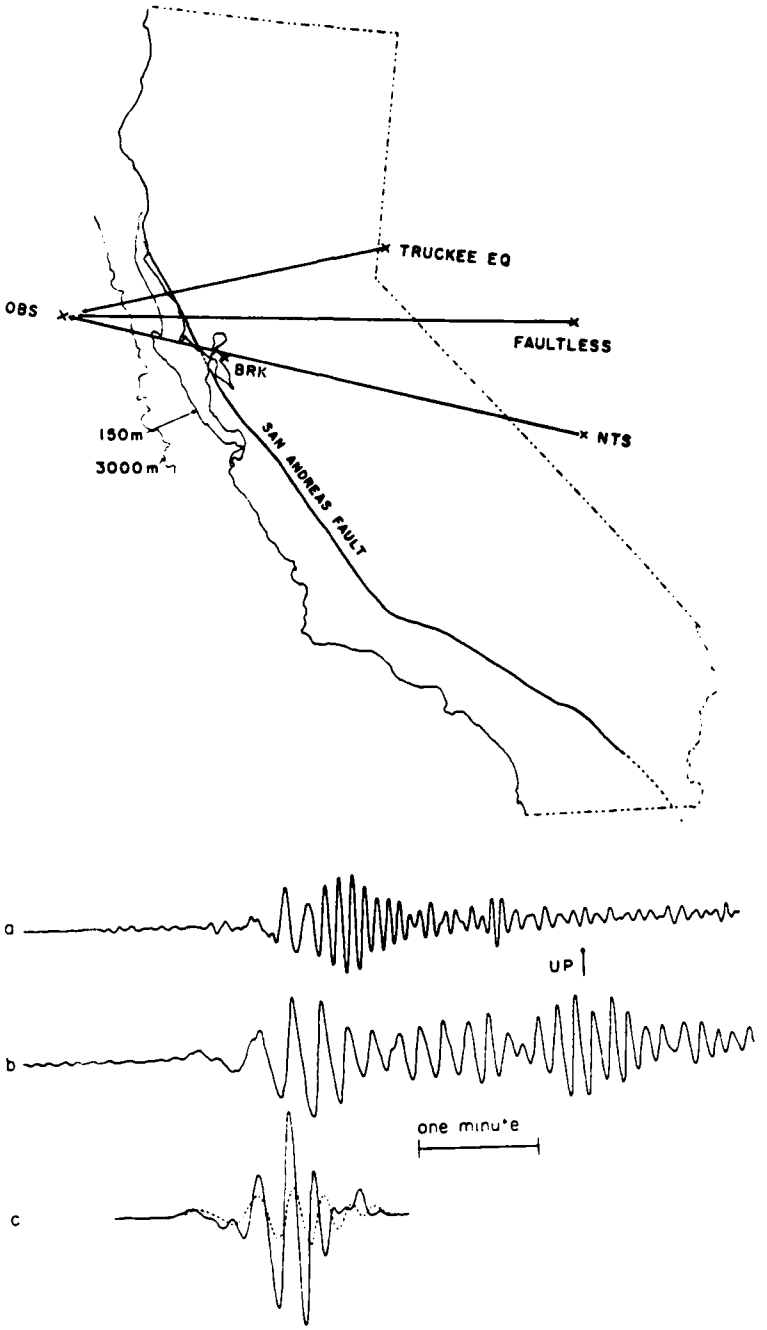
TRUCKEE EQ
OBS
FAULTLESS
BRK
NTS
150m
3000m
SAN ANDREAS FAULT
a
UP
b
one minute
c

Figure 2.

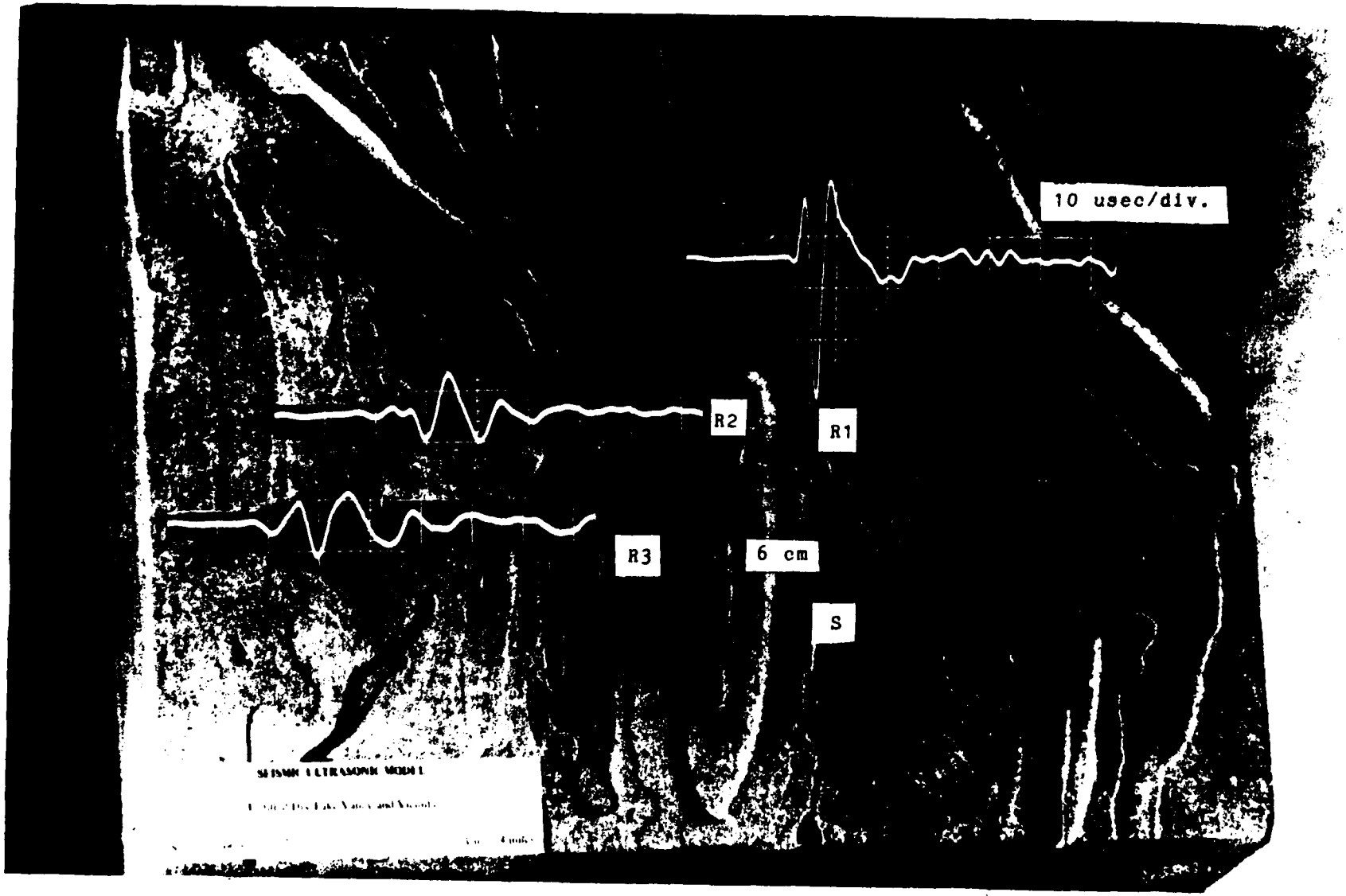

Figure 3.

II. TWO-DIMENSIONAL ULTRASONIC EXPERIMENTS AND FINITE DIFFERENCE CALCULATIONS

II.1. *LABORATORY STUDIES OF SURFACE SCATTERING*

Two and three-dimensional ultrasonic laboratory experiments have been carried out on the scattering of Rayleigh waves from surface topographic and structural heterogeneities. Two dimensional experiments were done using nickel and aluminum plates with topographic discontinuities modeled as steps, ramps, rectangular and triangular shaped "mountains" (Nathman, 1980; Toksöz, 1983). These experiments extended the results of previous studies (de Bremaecker, 1958; Kato and Takagi, 1956; Knopoff and Gangi, 1960; Lewis and Dally, 1970; Martel *et al.*, 1977; Pilant *et al.*, 1964). Figures 4, 5 and 6 show examples of incident, reflected (back-scattered) and transmitted (forward-scattered) Rayleigh waves across up and downsteps and "mountains." Note that transmitted and reflected waves account for a small fraction of incident Rayleigh wave energy. A large fraction of Rayleigh wave energy is scattered into body waves. Figures 7a,b show the nature of body waves generated due to Rayleigh wave scattering at a step. Note that more energy is scattered into S waves and both P and S scattering patterns are complex.

II.2 *FINITE DIFFERENCE MODELING OF SURFACE WAVE SCATTERING*

To investigate details of the scattering process, two-dimensional finite difference calculations are carried out for Rayleigh waves incident on topographic steps (Toksöz, 1983; Fuyuki and Nakano, 1984; Stephen *et al.*, 1985). In a perfectly elastic, two-dimensional, homogeneous, isotropic medium, the wave propagation for displacement $\underline{u}$ can be written

$$\underline{u}_{tt} = A_1 \underline{u}_{xx} + A_2 \underline{u}_{xz} + A_3 \underline{u}_{zz} \qquad (1)$$

where the displacement vector $\underline{u}$ equals

$$\underline{u} = (u(x,z,t) , w(x,z,t))$$

and

$$A_1 = \begin{bmatrix} \alpha^2 & 0 \\ 0 & \beta^2 \end{bmatrix} ,$$

$$A_2 = \begin{bmatrix} 0 & \alpha^2-\beta^2 \\ \alpha^2-\beta^2 & 0 \end{bmatrix} ,$$

$$A_3 = \begin{bmatrix} \beta^2 & 0 \\ 0 & \alpha^2 \end{bmatrix}$$

where α and β are P and S wave velocities. The boundary conditions for the free surface are the vanishing normal and shear stresses. These conditions can be represented in the case of an horizontal free surface by

$$\underline{u}_x + B_1 \underline{u}_z = 0 \qquad (2)$$

and in the case of a vertical free surface by

$$\underline{u}_x + B_2 \underline{u}_z = 0 \qquad (3)$$

where

$$B_1 = \begin{bmatrix} 0 & 1 \\ 1-2(\beta/\alpha)^2 & 0 \end{bmatrix}$$

$$B_2 = \begin{bmatrix} 1 & 1-2(\beta/\alpha)^2 \\ 0 & 0 \end{bmatrix}$$

The finite difference method is used to solve equation (1) subject to the boundary conditions (2) and (3) and to the initial conditions which will be described later. The procedure followed is similar to that used by Fuyuki and

Matsumoto (1980), and Munasinghe and Farnell (1973).

For the case of propagation in an infinite homogeneous media, the explicit finite difference formulation is stable only if:

$$\Delta t \leq \frac{\min(\Delta x, \Delta z)}{\sqrt{(\alpha^2+\beta^2)}} \tag{4}$$

when Δx and Δz are the grid dimensions in the horizontal and vertical directions and Δt is the timestep. The principal cause of inaccuracy in finite difference calculations in slowly varying media is grid dispersion. If the grid increments (Δx, Δz) are too large, low frequencies will travel faster across the grid than high frequencies, causing apparent dispersion. This result is generally true for compressional waves. For shear waves the dispersion relation is more complex. For some values of Poisson's ratio and propagation direction high frequencies may travel faster than low frequencies (Bamberger *el al.*, 1980; Trefethen, 1982; Sato and Ishihara, 1983). Care was taken to assure that both of the potential problems were correctly handled.

In our calculations we generate the initial Rayleigh wave with its eigenvelocity v_R. The incident waveform is chosen so that the vertical displacement w on a free surface has the shape of a Ricker wavelet (Ricker, 1953). The waveform in the wavenumber spectrum is

$$S(k)=(k/k_0)^2\exp[1-(k/k_0)^2] \tag{5}$$

where k_0 denotes the wavenumber corresponding to the maximum amplitude, and the dominant wavelength λ_0 is defined by $\lambda_0=2\frac{\pi}{k_0}$. This waveform has been used before by Munasinghe and Farnell (1973), and Fuyuki and Matsumoto (1980). To eliminate the edge effects, absorbing boundaries were placed at the sides and the bottom of the model following the formulation of Clayton and Engquist (1977) and Reynolds (1978).

In order to simulate laboratory models, the finite difference calculations are carried out using the model parameters with P wave velocity 6 km/sec, S wave velocity 3.46 km/sec and Rayleigh wave velocity 3.18 km/sec. This case corresponds to a Poisson ratio of 0.25. The center frequency of the wavelet is 0.318 MHz and the corresponding wavelength is 10 mm. In numerical modeling we use 25 grid points per wavelength, which gives $\Delta x = \Delta z = 0.4$ mm. The Δt value is 0.047 μ sec.

The ultrasonic models have corners at 90° and 270° angles. A partially off-centered finite difference scheme has been employed by other authors (Alterman and Rotenberg, 1969; Munasinghe and Farnell, 1973; Fuyuki and Matsumoto, 1980) to deal with such corners. The first two methods give an accuracy of the order of Δx, and the Fuyuki and Matsumoto method an accuracy on the order of $(\Delta x)^2$. Fuyuki and Matsumoto (1980) and Fuyuki and Nakano (1984) show that the relative error in finite difference calculations is ± 1 per cent for the horizontal and vertical displacements located close to the free surface. Below one wavelength the relative errors increase to about ±4 per cent. Since we follow the same approach as Fuyuki and Matsumoto, the accuracy of our calculations should be similar to the above values.

In order to separate the scattered P and S waves, the divergence ($\nabla . \underline{u}$) and curl ($\nabla \times \underline{u}$) of the displacement field is calculated at each point at designated times. Figures 8 and 9 show snapshots of the motion at different times for Rayleigh waves incident on a downstep and upstep surface discontinuity. Note that the dilatation component of the scattered field is much smaller than the rotational. The complex patterns of scattering of Rayleigh to P and S, and in turn the scattering of body waves are clearly shown in these color figures. These results show in greater detail what was observed in the laboratory experiments (Figures 4, 5, 6, 7a, and 7b).

A case of special interest is the Rayleigh wave scattering from a rectangular surface feature (i.e., a mesa). The experimental results showed that two Rayleigh waves are generated by the mesa: the first by the Rayleigh-shear-Rayleigh scattering, the second by Rayleigh wave transmission following the surface contour (Figure 6, especially second trace from bottom).

Finite difference calculations for this case are shown in Figures 10 and 11. Figure 10 shows the particle displacement vectors. Frames c, d, e, and f show how Rayleigh-shear-Rayleigh scattering takes place. The complexity of displacements due to interference in the mesa is clearly illustrated. In Figure 11, the curl of displacement (shear strain) on the right hand side demonstrates a case of Rayleigh-shear-Rayleigh scattering. Rayleigh waves "transmitted" by this mechanism are larger than Rayleigh waves that follow the surface.

In summary, these two-dimensional results demonstrate that high frequency surface wave propagation across topographic irregularities can be complex. Multiple scattering between Rayleigh and body waves can take many forms based on topography and wavelength. In the next section we show the results from simple three-dimensional models.

REFERENCES

Alterman, Z. and A. Rotenberg, 1969. Seismic waves in a quarter plane. *Bull. Seism. Soc. Am.*, *59*, 347-368.

Bamberger, A., G. Chavent and P. Lailly, 1980. Etudes de schemas numeriques pour les equations de l'elastodynamique lineaire. *Rapports de Recherche*, *41*, INRIA, B.P. 105, 78150 Le Chesnay, France.

de Bremaecker, J.-Cl., 1958. Transmission of a reflection of Rayleigh waves by corners, *Geophysics*, *23*, 253-266.

Clayton, R. and B. Engquist, 1977. Absorbing boundary conditions for acoustic and elastic wave equations, *Bull Seism. Soc. Am.*, *67*, 1529-1540.

Fuyuki, M. and Y. Matsumoto, 1980. Finite difference analysis of Rayleigh wave scattering at a trench, *Bull. Seism. Soc. Am.*, *67*, 1529-1540.

Fuyuki, M. and M. Nakano, 1984. Finite difference analysis of Rayleigh wave transmission past an upward step change, *Bull. Seism. Soc. Am.*, *74*, 893-911.

Kato, Y. and A. Takagi, 1956. Model seismology (part 3): Wave propagation in the step-shaped structure and on the cliff, Sci. Rep. Tohoku Univ., ser. 5.8, 74-86.

Knopoff, L. and A. Gangi, 1960. Transmission and reflection of Rayleigh waves by wedges, *Geophysics*, *25*, 1203-1214.

Lewis, D. and J.W. Dally, 1970. Photoelastic analysis of Rayleigh wave propagation in wedges, *Geophysics*, *35*, 3387-3398.

Martel, L., M. Munasinghe and G.W. Farnell, 1977. Transmission and reflection of Rayleigh waves through a step, *Bull. Seism. Soc. Am.*, *67*, 1277-1290.

Munasinghe, M. and G.W. Farnell, 1973. Finite difference analysis of Rayleigh wave scattering at vertical discontinuities, *Jour. Geophys. Res.*, *78*, 2454-2466.

Nathman, D.R., 1980. Rayleigh Wave Scattering Across Step Discontinuities, M.S. Thesis, Massachusetts Institute of Technology, Cambridge, MA.

Pilant, W.L., L. Knopoff and F. Schwab, 1964. Transmission and reflection of surface waves at a corner, 3. Rayleigh waves (experimental), *Jour. Geophys. Res.*, *69*, 291-298.

Reynolds, A.C., 1978. Boundary conditions for the numerical solution of wave propagation problems, *Geophysics*, *43*, 1099-1110.

Ricker, N., 1953. The form and laws of propagation of seismic wavelets, *Geophysics*, *18*, 10-40.

Sato, Y. and K. Ishihara, 1983. On the numerical calculation of wave propagation by the finite difference method, *Bull. Earthq. Res. Inst.*, *58*, 163-173.

Stephen, R.A., F. Pardo-Casas and C.H. Cheng, 1985. Finite-difference synthetic acoustic logs, *Geophysics*, in press.

Trefethen, L., 1982. Wave Propagation and Stability for Finite Difference Schemes, Ph.D. Thesis, Stanford University, Stanford, CA.

Toksöz, M.N., 1983. Development of ultrasonic modeling techniques for the study of crustal inhomogeneities. Final Report to Air Force Geophysics Laboratory, AFGL-TR-83-0070.

FIGURE CAPTIONS

Figure 4. Seismograms of reflected and transmitted two-dimensional Rayleigh wave pulses incident on an upstep.

Figure 5. Seismograms of reflected and transmitted two-dimensional Rayleigh waves incident on a downstep.

Figure 6. Seismograms of reflected and transmitted pulses for rectangular "mountains" with different geometries.

Figure 7a. Receiver positions used to measure azimuthal scattering of step (two-dimensional).

Figure 7b. Seismograms taken at receiver positions as shown on Figure 7a.

Figure 8a,b,c. Time sequence of divergence (left side) and curl (right side) of displacement for Rayleigh wave incident on a downstep.

Figure 9. As for Figure 8, but for upstep.

Figure 10a-i. Time sequence of displacement vectors depicting the scattering of a surface wave for the rectangular "mountain" case. See text for discussion.

Figure 11a,b. As for Figure 8, but for a rectangular "mountain".

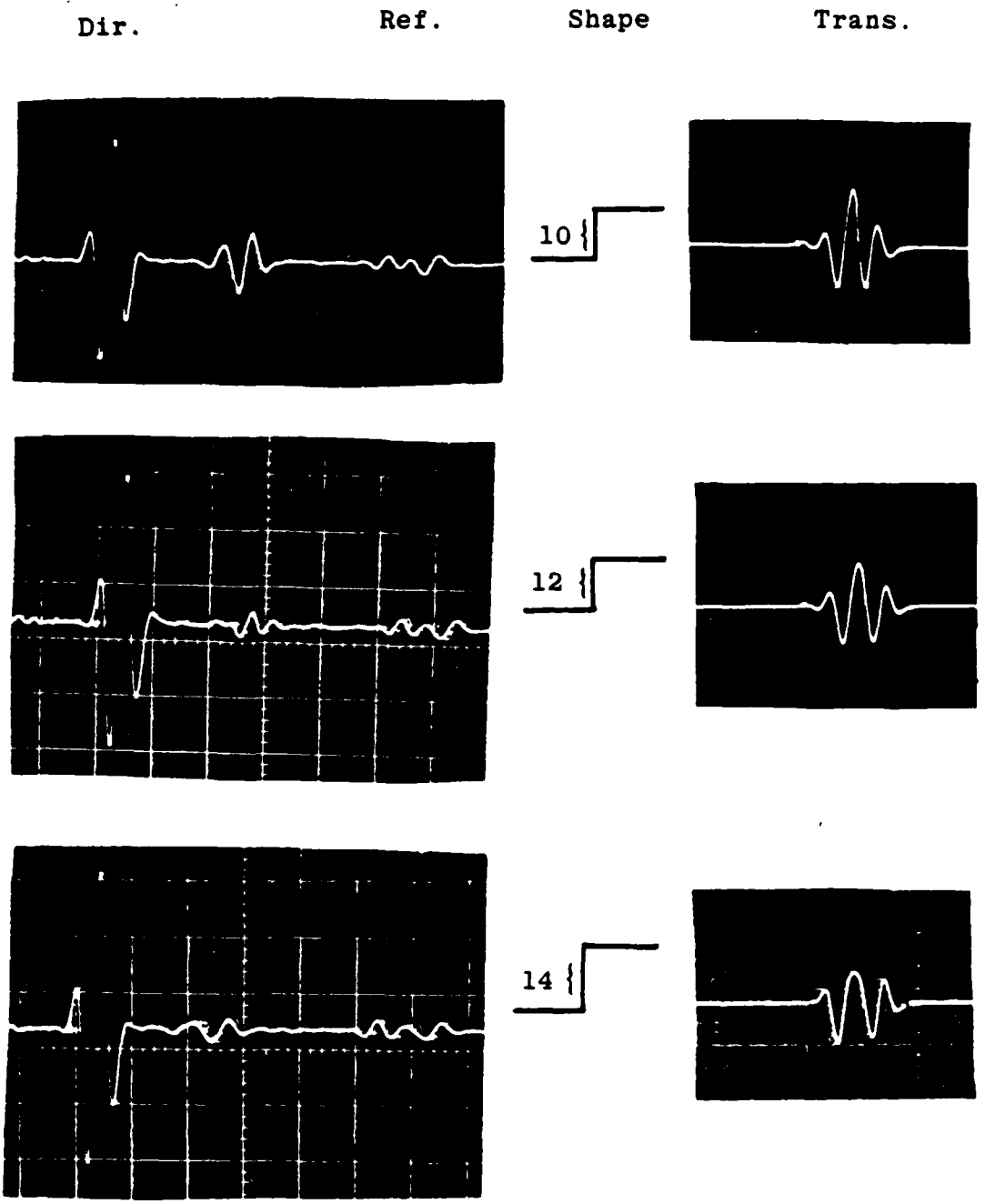

Figure 4.

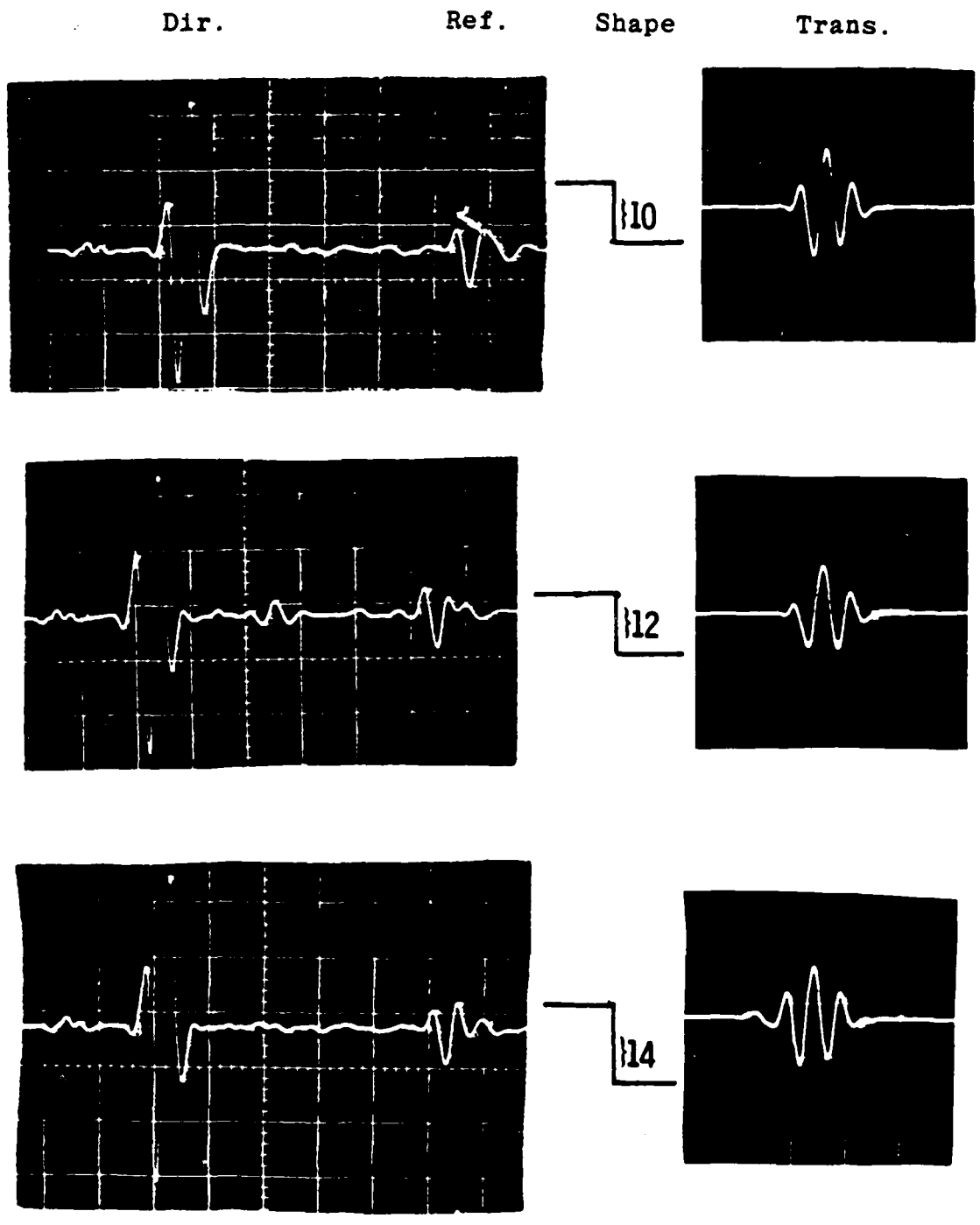

Figure 5.

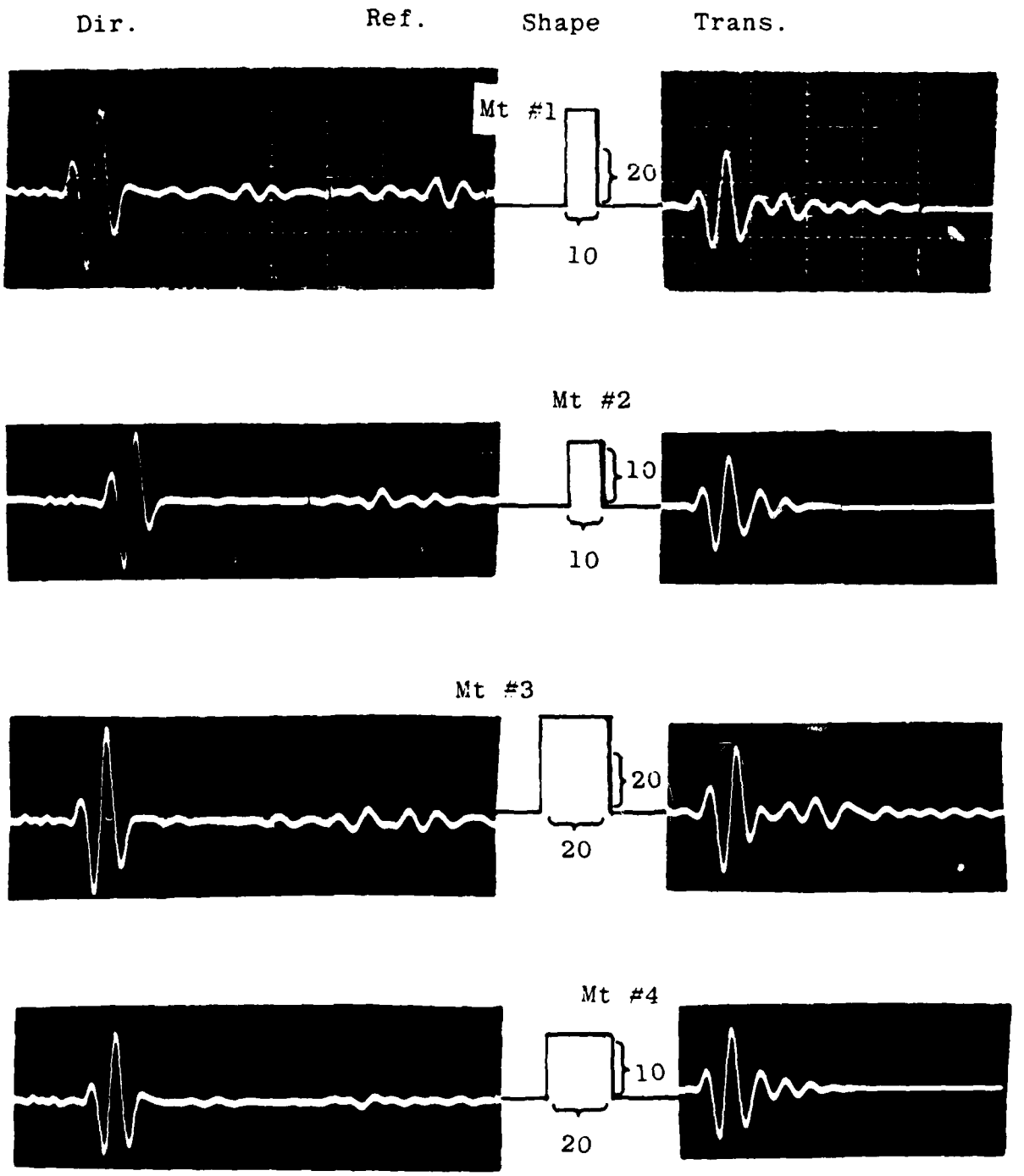

Figure 6.

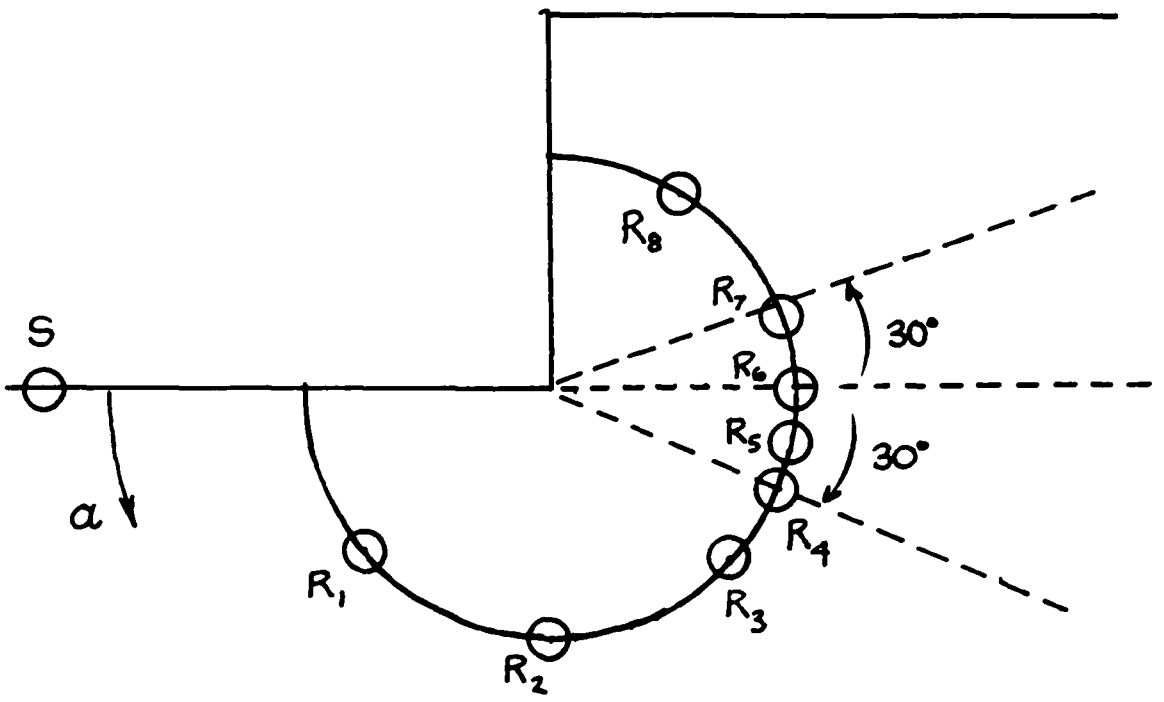

Figure 7a.

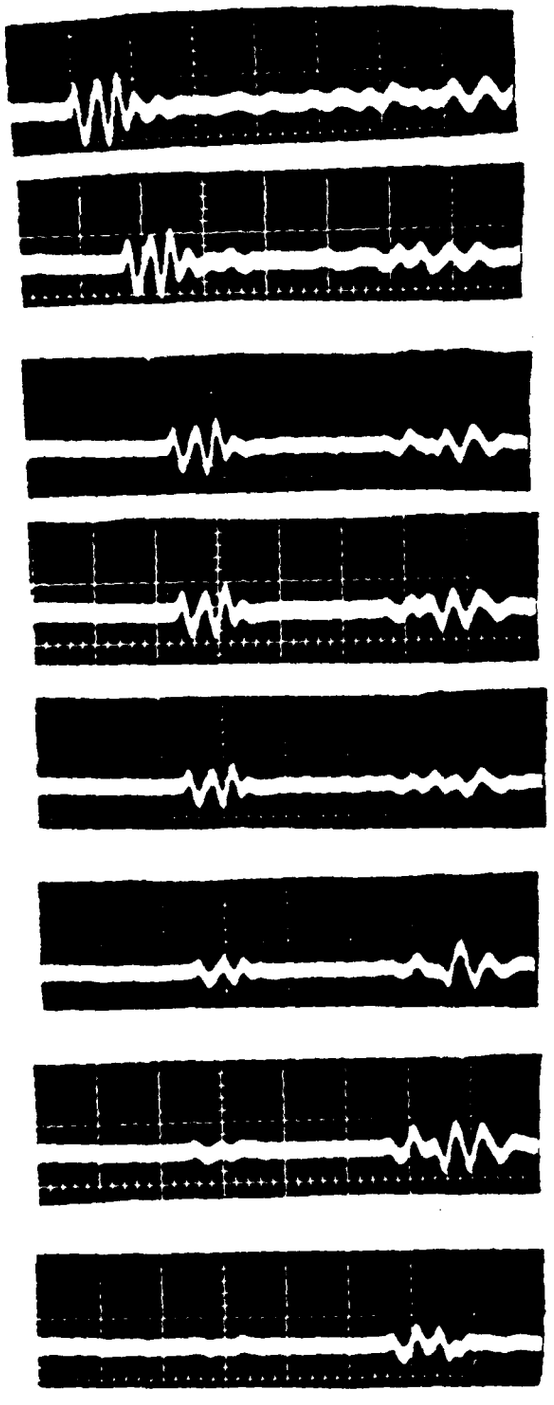

R_n	α°	Distance (mm)
R_1	45°	165
R_2	90°	205
R_3	135°	237
R_4	150°	243
R_5	162.5°	247
R_6	180°	249
R_7	207°	245
R_8	237°	230

Figure 7b.

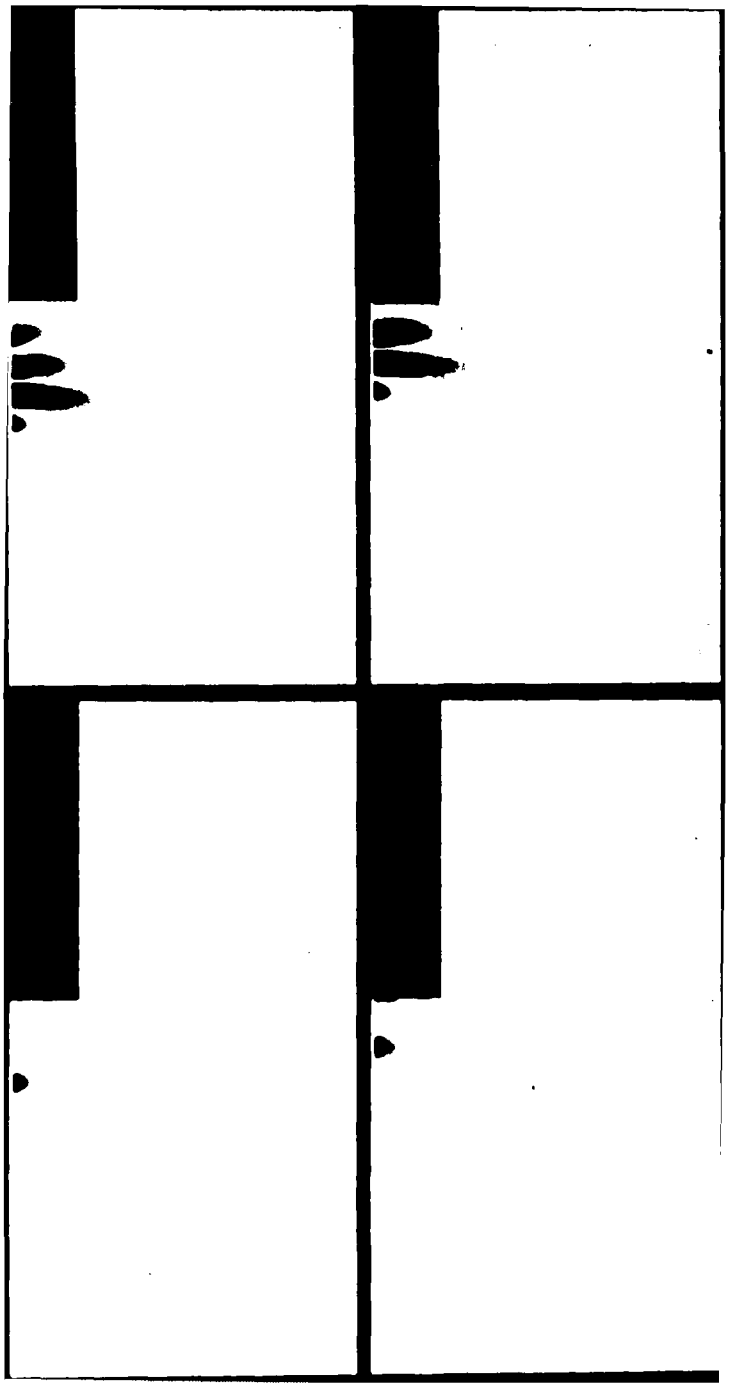

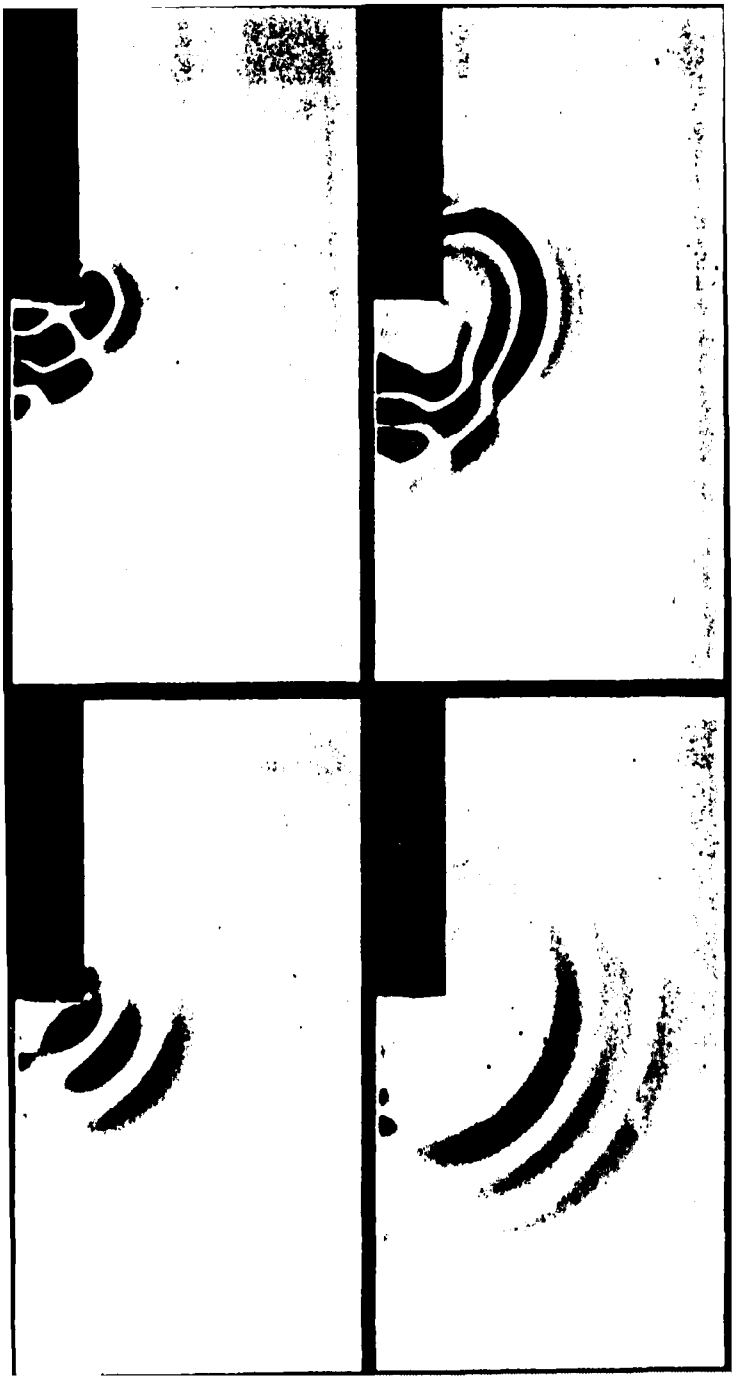

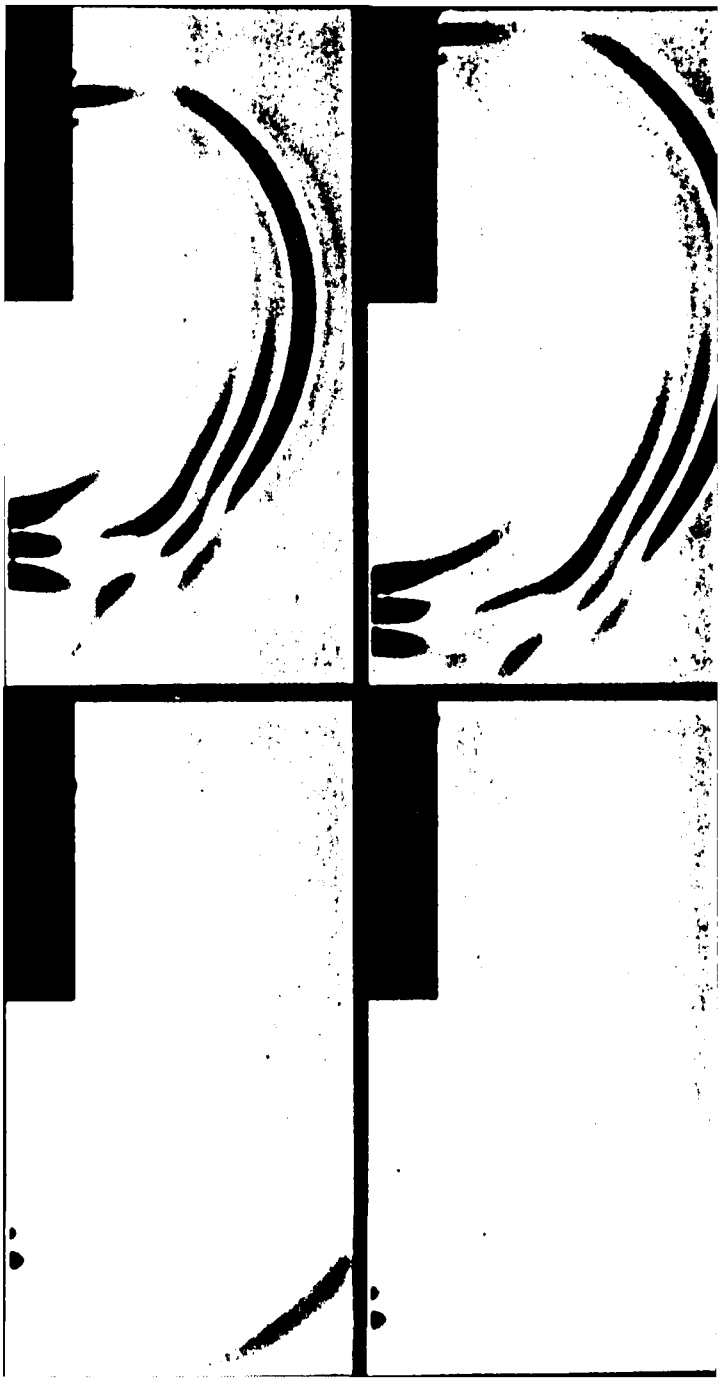

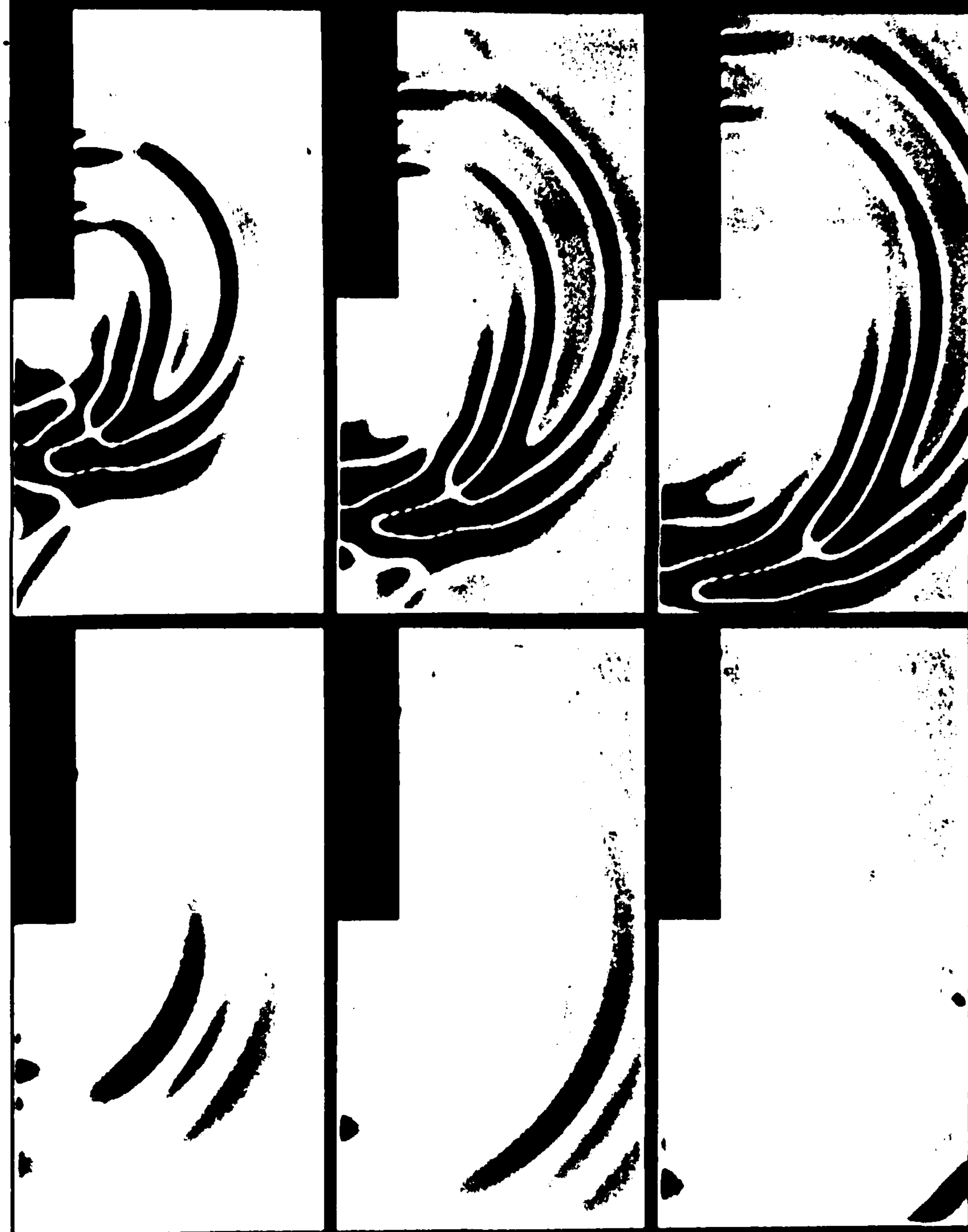

T-100

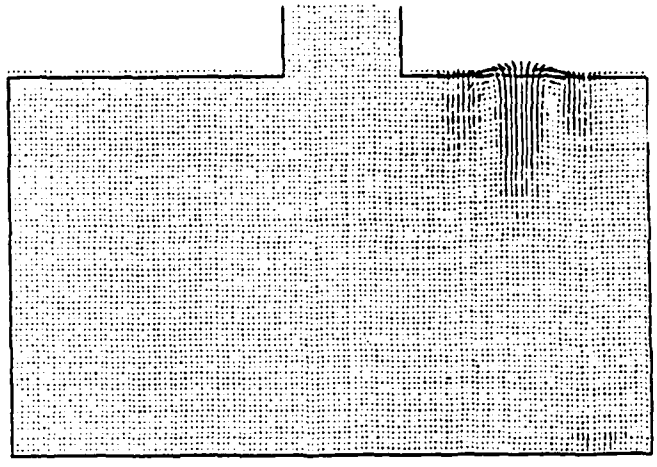

a

T-200

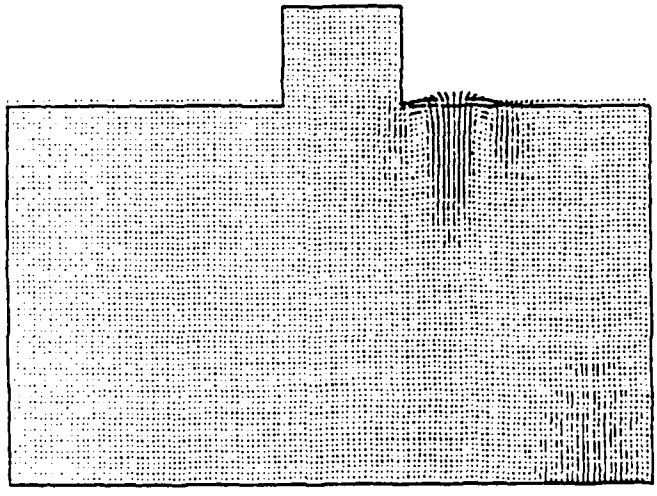

b

T-300

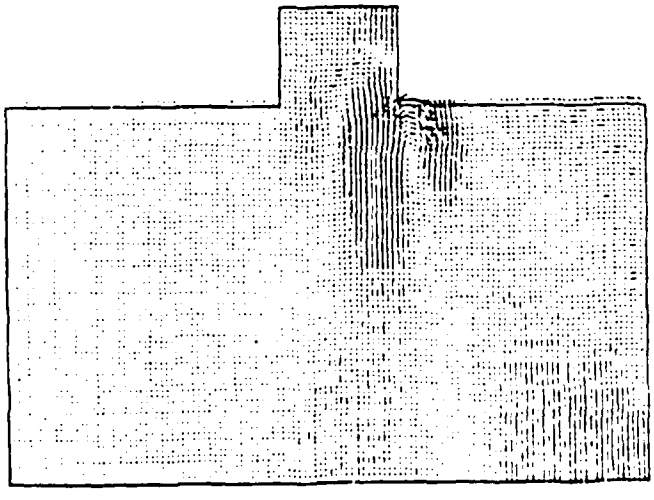

c

Figure 10 a-c

T-400

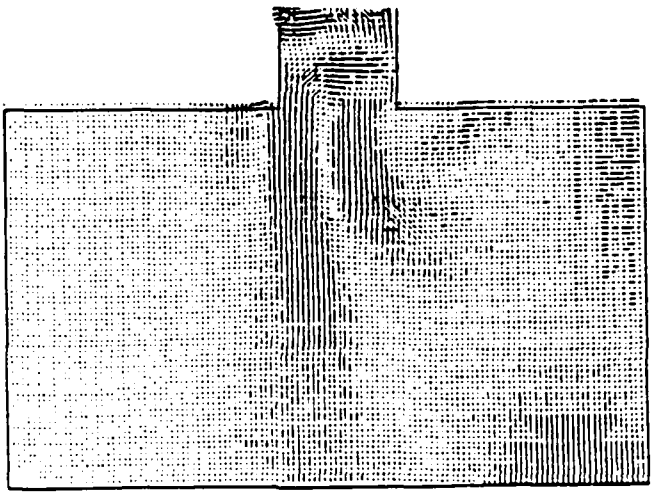

d

T-500

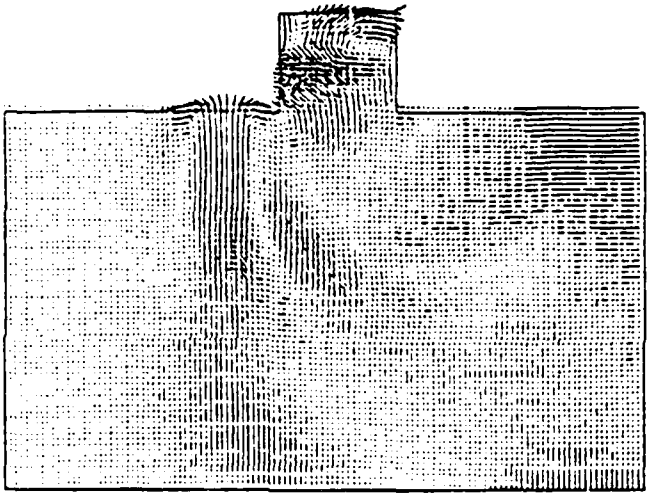

e

T-600

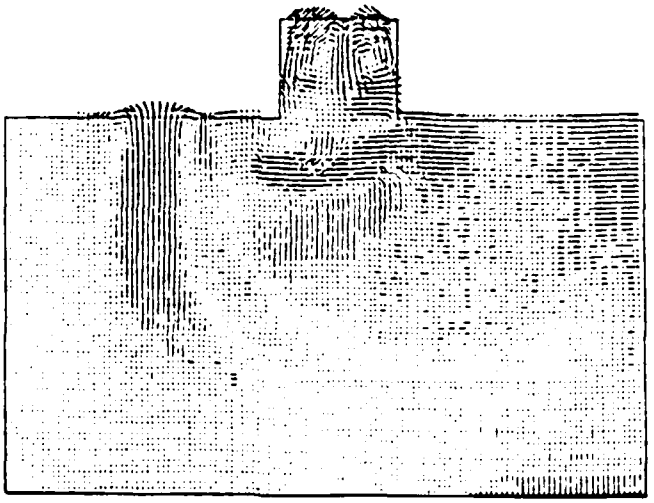

f

Figure 10 d-f

T-700

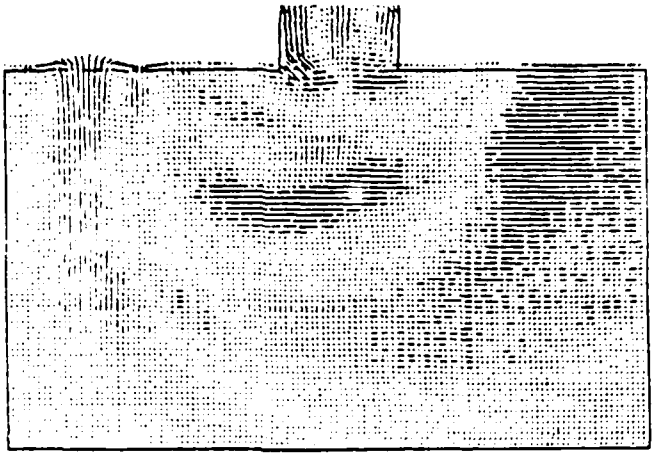

g

T-800

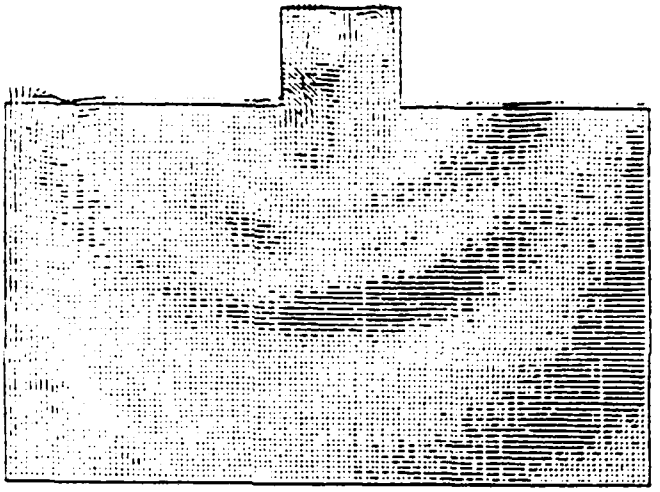

h

T-900

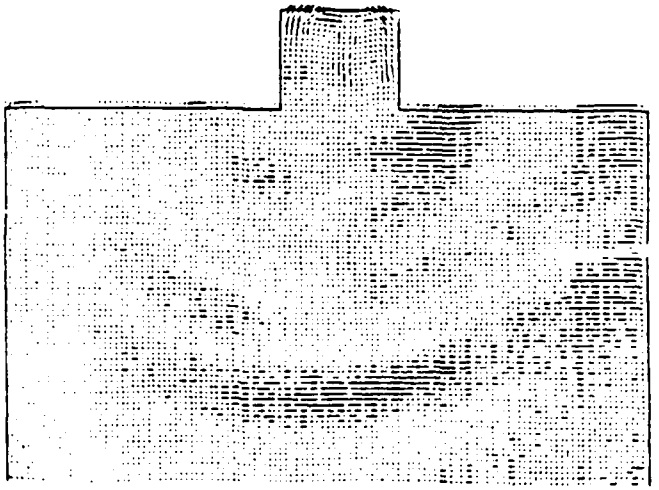

i

Figure 10 g-i

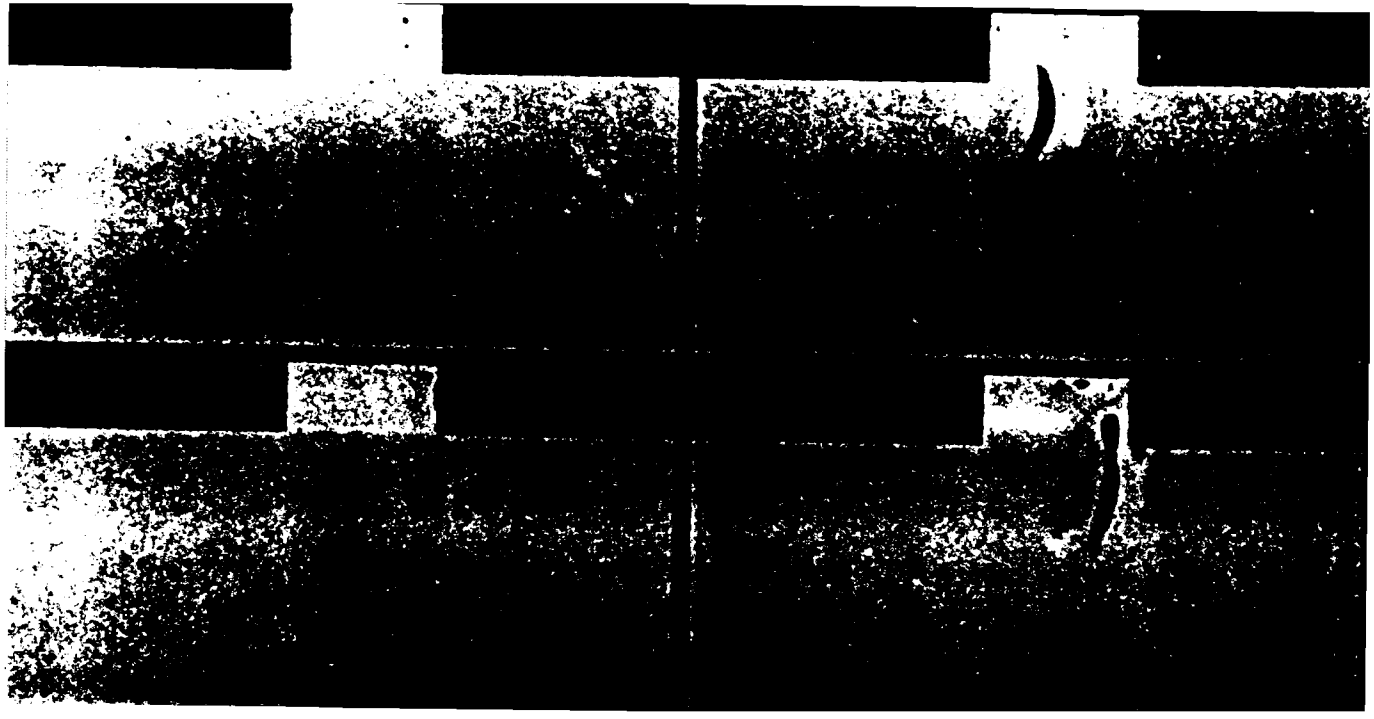

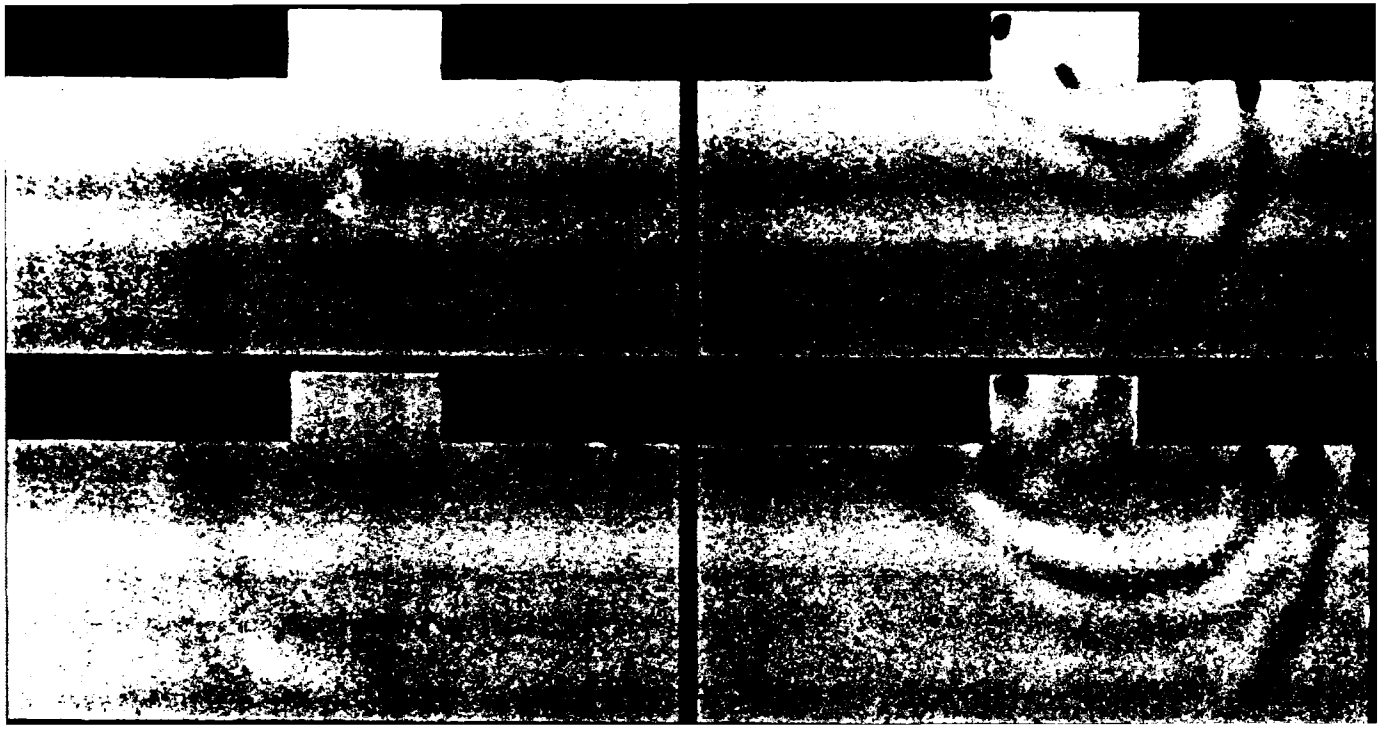

III. THREE DIMENSIONAL EXPERIMENTS

III.1 *INTRODUCTION*

Rayleigh wave propagation in strongly-varying structures is a complex process well suited to analysis by ultrasonic modeling methods. Until recently, ultrasonic modeling of surface wave transmission and scattering has been limited to two dimensions. In this chapter we report on a series of ultrasonic modeling experiments investigating the propagation and scattering of Rayleigh waves by simple three-dimensional topographic features.

Rayleigh waves propagating in two dimensions through simple steps or around corners and in wedges have been studied experimentally by a number of investigators (de Bremaecker, 1958; Kato and Takagi, 1956; Lewis and Dally, 1970; Knopoff and Gangi, 1960; Pilant *et al.*, 1964; Martel *et al.*, 1977; and Nathman, 1980). Detailed 'snapshots' of the complete stress field of Rayleigh waves scattered in wedges have been obtained using photoelastic methods (Lewis and Dally, 1970). Chapter II of this report presents our results.

Development of theoretical and numerical methods of synthesizing Rayleigh waves scattered from simple structures has typically lagged behind experimental results. Rayleigh wave transmission and reflection coefficients across vertical boundaries in two dimensions have been calculated using approximate variational methods (e.g. McGarr and Alsop, 1967). Recently, synthesis of complete seismograms of Rayleigh waves reflected from, and transmitted through, a vertical step has been performed using the finite-difference method (Toksöz 1983; Fuyuki and Nakano, 1984; Chapter II). In three dimensions, numerical computations are limited. Approximate methods to estimate transmission and reflection coefficients of Rayleigh waves incident at steep angles on a vertical boundary have, however, been successfully applied (Malichewsky, 1976; Chen and Alsop, 1979).

Scattering of Rayleigh waves in three dimensions can be investigated in the laboratory using ultrasonic methods. Rayleigh wave propagation in three-dimensions has already been studied using realistic three-dimensional scale models of surface topography (e.g. Toksöz, 1983). In such models, however, even a simple input pulse is severely distorted by the complex structure. Subtle effects of topography on Rayleigh wave propagation and scattering are thus easily obscured by the complexity of the model. An important step toward an understanding of surface wave scattering in three-dimensions is the investigation of propagation in simple models of canonical form. In this chapter, we investigate Rayleigh wave scattering from step and ramp-type topographic discontinuities and study their implications for surface wave propagation across major features such as ocean-continent boundaries and the Tibetan Plateau.

III.2 *EXPERIMENTAL METHOD*

The model used in this study consists of a solid block (200x200x100 mm^3) of aluminum. Steps of various height and geometry are milled into one of the large faces (Figure 12).

The ultrasonic source and receiver each consist of a 2.25 MHz P wave transducer coupled to a lucite wedge. P waves generated by the transducer propagate through the wedge and excite Rayleigh waves in the aluminum with high efficiency. Similarly, the transducer-wedge combination is an efficient Rayleigh wave sensor. The radiation pattern of the transducer-wedge combination is highly directional; at an angle of 10° from the axis of the central lobe, peak energy is reduced to less than 25% of the axial peak energy. The combination of these features makes the transducer-wedge combination especially useful when working with a low-loss medium such as aluminum; attenuation can be neglected in the analysis of Rayleigh wave propagation, and

the observed Rayleigh waves are uncontaminated by body waves multiply reflected at the edges of the model.

Peak energy of Rayleigh waves traveling on the aluminum block (V_p = 6.4 km/sec; V_s = 3.2 km/sec; c_R = 3.0 km/sec) lies in the range 0.2—2.0 MHz (λ=1.5—15 mm). In this frequency band the spectrum is repeatably obtained from a given model and source-receiver configuration. We therefore take this as the usable bandwidth of the modeling experiments. Because the model is essentially a half-space, only fundamental-mode Rayleigh waves are observed. Since a half-space is non-dispersive to Rayleigh waves, the half-space Rayleigh wave represents the impulse response of the transducers and recording system.

When a Rayleigh wave encounters a step some of the incident energy is transmitted through the step, some is reflected from the step, and some is converted to body waves (de Bremaecker, 1958; Knopoff and Gangi, 1960; Martel *et al.*, 1977; Toksöz, 1983). In general the efficiency of transmission through or reflection from a step depends on the wavelength relative to the step height (e.g. McGarr and Alsop, 1967). In order to facilitate comparison of models with different step heights, therefore, wavelengths are normalized to the step height. The "normalized frequency", $\hat{f}$, is obtained from the scaling relation

$$\hat{f} = \frac{hf}{c} = \frac{h}{\lambda} \qquad (6)$$

where f is the frequency, c is the phase velocity, λ is the wavelength, and h is the step height. For a given step height, the range of usable normalized frequencies is limited by the usable bandwidth of the modeling experiments. This is an important consideration when the model seismograms are scaled to correspond to real Earth seismograms. Transmission and reflection coefficients calculated from Rayleigh waves traveling across steps of various heights indicate that the model scaling relation (Equation 6) is generally appropriate over a wide range of frequencies and step heights.

We define the the Rayleigh wave energy transmission coefficient, E_T, as

$$E_T(\hat{f}) = \left[\frac{A_T(\hat{f})}{A_0(\hat{f})}\right]^2, \tag{7a}$$

where $A_T(\hat{f})$ is the Fourier amplitude spectrum of the transmitted Rayleigh wave, and $A_0(\hat{f})$ is the amplitude spectrum of the Rayleigh wave propagating across the aluminum half-space. The reflection coefficient, E_R, is defined in an exactly analogous way:

$$E_R(\hat{f}) = \left[\frac{A_R(\hat{f})}{A_0(\hat{f})}\right]^2, \tag{7b}$$

where $A_R(\hat{f})$ is the amplitude spectrum of the reflected Rayleigh wave.

Transmitted Rayleigh waves are recorded by keeping source and receiver at opposite points on the diameter of a circle centered on the step (see Figure 12). Reflected waves are observed by placing source and receiver at equal angles from the normal to the strike of the step. Incidence angle is measured from the strike of the step.

III.3 *MODELING RESULTS*

Vertical Step Model

Figure 13 shows seismograms of Rayleigh waves transmitted across a 3 mm vertical step at incidence angles ranging from 15° through 90° (normal incidence). The small signal arriving about 1 μsec before the Rayleigh wave is an S wave excited at the step. At a given incidence angle the waveforms for the case of upstep and downstep transmission are essentially identical. Note that not only do peak amplitudes decrease by a factor of two to four or more, but also that the waveform changes strongly as a function of angle of incidence. At normal incidence (Θ=90°) transmission coefficients (Figure 14) agree well with those obtained for a two-dimensional step using theoretical (numerical)

calculations (Drake, 1972; Martel *et al.*, 1977; Fuyuki and Nakano, 1984).

At normal incidence the fraction of transmitted energy (E_T) seldom exceeds 20% within the usable frequency band. This represents a loss of over 80% of the incident Rayleigh wave energy to reflected surface waves and converted body waves.

Reflected Rayleigh wave seismograms are complicated by the presence of double reflections, separated by about 2 μsec (Figure 15). In Figure 15a, the first reflection corresponds to the Rayleigh wave reflected from the bottom edge of the step, the second to the Rayleigh wave reflected from the upper edge after propagating up the face of the step. These are further complicated by multiple scattering and Rayleigh to shear scattering. Reflections from a downstep (Figure 15b) are much larger than those from an upstep (Figure 15a). Also, shapes of down-step reflected waveforms are different from those of upstep. They do not exhibit the strong incidence angle dependence. Similar differences between upstep and downstep scattering of Rayleigh waves have been observed in two-dimensional modeling experiments (e.g. Nathman, 1980; Chapter II).

In general the reflected energy is very small, particularly at normal or near-normal incidence (Figure 17). At most angles and frequencies, reflected energy accounts for no more than 10-20% of the incident energy. As the incidence angle becomes more grazing the reflected energy increases rapidly, especially for wavelengths approximately equal to three times the step height ($\hat{f} \approx 0.3$).

It is clear from Figures 14 and 16 that the efficiency of body wave scattering is strongly dependent on the angle of incidence. In the 3 mm step model, at wavelengths equal to one-half the step height (the first maximum in Figure 14) about 90% of the incident energy is scattered to body waves. As the

incidence angle decreases to near 0° (grazing incidence), this figure drops to about zero.

Ramp Model

To investigate the effect of a more gradual change of elevation, the 3 mm step was tapered to a slope of 60° from the horizontal (see Figure 12). Distortion of both transmitted and reflected waveforms is strong, particularly at normal and near-normal incidence (Figure 17).

Energy transmission coefficients for this model (Figure 18a) are generally higher than those for the step model (Figure 14b) at frequencies below $\hat{f} \approx 0.5$. The energy minimum near $\hat{f} \approx 0.9$ at normal incidence is considerably smaller than the corresponding minimum for the step model. Reflected energy (Figure 18b) is considerably smaller than for the case of the vertical step (Figure 14a). The double reflection is, however, apparent at all angles. Interference between the two reflections and the scattered body waves contributes to the complexity of the seismograms.

Note that in the case of the ramp model the frequencies have been normalized to a step height of h=3.0 mm; in fact this normalization is arbitrary. While the vertical change in elevation is indeed 3.0 mm, the distance from the lower edge to the upper edge as measured along the ramp surface is actually larger than this ($\frac{h}{\sin\alpha}$, where α is the ramp angle). This distance may also enter into the scaling relations. Direct comparisons between step and ramp transmission and reflection coefficients may not, therefore, be appropriate when scaled to the same step height.

Azimuthal Dependence of Scaling

In the models discussed above, the character of the transmitted and reflected waveforms changes most rapidly as the incidence angle decreases

below about 30^{o}. It is in the range 0^{o} to 30^{o} that the behavior of Rayleigh wave propagation departs most strikingly from that predicted by two-dimensional theoretical and approximate methods. At incidence angles greater than 30° simple empirical relations can be found between the results obtained at normal and oblique incidence.

In the case of transmission through the vertical step (Figure 14), note that the energy transmission minimum near $\hat{f}$=0.5 at normal incidence moves to higher frequency as the incidence angle decreases. The equivalent effect is observed for normally incident waves when the step height is decreased. This suggests that the effective step height is dependent on incidence angle. That is, as the incidence angle decreases the incident Rayleigh wave "sees" a shorter step. The functional dependence of effective step height on incidence angle is estimated by finding a simple functional relation between incidence angle and a particular feature in the transmission curves. The normalized frequency at which the first minimum occurs in the transmission curves is approximated well using the empirical relation

$$\hat{f}_{min}(\Theta) = \frac{\hat{f}_{min}(90^{\circ})}{\sin\Theta}, \tag{8a}$$

where $\hat{f}_{min}(\Theta)$ is the value of $\hat{f}$ at which the first minimum in the transmission curve appears. When this relation is applied to the entire transmission curve the curves at each incidence angle can be made to coincide (Figure 19). In terms of the effective step height at angle Θ, Equation (8a) implies

$$h_{eff}(\Theta) = h\sin\Theta \tag{8b}$$

To a first approximation the transmission coefficient for an arbitrary incidence angle can thus be estimated from the normal incidence transmission coefficient using this empirical relation. This approximation is poor, however, at incidence angles shallower than about 30°.

Because of its strong incidence angle dependence, the reflection coefficient for the step is difficult to model with a simple empirical relation.

III.4 *IMPLICATIONS FOR THE EARTH*

One of the most interesting features of the ultrasonic results is that both transmitted and reflected Rayleigh wave pulse shapes are severely altered as a result of interaction with the various steps. The waveform distortion is due to the combined effects of frequency-dependent energy transmission and reflection and interference of waves multiply reflected within the step. More complicated input signals, such as dispersive wave trains, can be expected to undergo similar kinds of angle-dependent waveform distortion after propagating across a step.

The effect of a given model on a surface wave signal is determined by convolving the desired input signal with the impulse response of the model. As noted earlier, the Rayleigh wave propagating across the aluminum half-space represents the impulse response of the transducers and recording system. The impulse response of a given model for waves propagating in a given direction is thus the result of deconvolving the transducer/recording system impulse response from the recorded signal. In the frequency domain we may write

$$\hat{T}_m(\Theta;\omega) = \frac{\hat{S}_m(\Theta;\omega)}{\hat{S}_{hs}(\omega)} \quad , \tag{9}$$

where $\hat{T}_m(\Theta;\omega)$ is the complex transfer function for the desired model at incidence angle Θ, $\hat{S}_m(\Theta;\omega)$ is the complex Fourier spectrum of a Rayleigh wave propagating across the model at angle Θ, $\hat{S}_{hs}(\omega)$ is the half-space Rayleigh wave spectrum, and ω is the angular frequency. The inverse Fourier transform of this quantity yields the impulse response of the given model.

As a test of the effect of a step on a dispersed wave train, a chirped sinusoid was convolved with the impulse response of the 3 mm vertical step and ramp models at several incidence angles (Figure 20). At some incidence angles and frequencies the envelope of the wave train drops to near zero, suggestive of the "beating" phenomenon frequently observed in seismograms of Rayleigh waves propagating across ocean basins. This beating is usually attributed to multipathing due to lateral heterogeneities along the propagation path (Evernden 1953,1954). At least part of the amplitude modulation of dispersed Rayleigh wave trains observed in the Earth may be due to propagation across sharp structural features such as those modeled here.

In order to investigate the effect of simple steps on Rayleigh wave propagation in the Earth, the physical dimensions of the model are scaled to correspond with those of some realistic Earth structure. The scaling factor relating the physical dimensions of the Earth to those of the model is given by the linear relation (White, 1965):

$$T_m = kT_e. \tag{10}$$

where the scaling factor k is given by

$$k = (\frac{L_m}{L_e})(\frac{V_e}{V_m}),$$

and T_χ, L_χ, and V_χ are characteristic times, lengths, and velocities, respectively in either the model (m) or the Earth (e).

In general, the terrestrial scale length appropriate for a given physical problem is considerably greater than that which would be indicated by surface topography alone. In discussions of terrestrial scaling, the terrestrial scale length is not to be interpreted literally as the dimension of any real structure; it is simply the characteristic dimension of a highly simplified model. The topographic expression of the physical model includes the combined effects of terrestrial topography and deep structure. The ultrasonic step models

described in the first section of this chapter represent a very simplified approximation to complex boundaries of vertical heterogeneities of the earth structure. It is still worthwhile, however, to investigate whether models produce effects similar to those observed in the earth.

We take as the input signal for a given model a real or synthetic terrestrial seismogram. The seismogram is resampled at a rate determined by the model scaling factor, and convolved with the impulse of the model. The result of the convolution is resampled to restore the seismogram to its original (terrestrial) time scale.

Because the usable frequency of Rayleigh waves in the modeling experiments is limited to the band 0.2—2.0 MHz, the range of normalized frequencies available for scale modeling is also limited. The range of step heights and wavelengths which may be modeled reliably given the band-limited nature of the ultrasonic pulse is shown in Figure 21.

The Ocean-Continent Margin

The incidence angle dependence of Rayleigh wave transmission across the ocean-continent margin can be seen in recordings of teleseismic oceanic Rayleigh waves made at coastal stations. For example, Figure 22 shows Rayleigh waves recorded at WWSSN stations on the west coast of the United States from an earthquake in the Loyalty Islands. The incidence angle is taken to be the angle between the great-circle path and the continental shelf. For paths to BKS, COR and LON, the angles are approximately 90°, 60°, and 45°, respectively. Among the continental stations in this example, epicentral distance ranges from 87.2° (BKS) to 91.9° (LON). Great-circle azimuths vary by no more than about 1° and source radiation patterns would have the same effect at these stations. Differences between the seismograms recorded at the continental

stations are therefore primarily due to variations in the incidence angle. At normal incidence (BKS) most of the Rayleigh wave energy is confined to the first dozen or so cycles, after which time the amplitude decays rapidly to a small value. As the incidence angle decreases to near-grazing, the initial 'packet' of energy broadens and the rate of amplitude decay decreases. This trend is consistent with that observed in the chirped sine synthetics (Figure 20).

Synthetic Rayleigh wave seismograms were generated for a pure oceanic path using the PEM-O model (Dziewonski *et al.*, 1975) and convolved with the impulse response of the 3 mm ramp models, scaled to a height of 60 km (Figure 22b). The model-synthetic seismograms exhibit azimuthal behavior similar to that of the real seismograms (Figure 22a).

In this example we have assumed the Rayleigh waves propagate on the great circle path between source and receiver. In fact, the velocity contrast across the ocean-continent margin in the Earth is such that Rayleigh waves of a given period traversing the margin will deviate from the great-circle path by an angle governed by Snell's law (e.g. Evernden, 1953; Capon, 1970). Using the coast and ocean models given by Drake and Bolt (1980) we find that, in the period range of interest in this example (15-40 sec), Rayleigh waves incident on the coast at incidence angles greater than 30° are refracted laterally by no more than about 6°. This is within the uncertainty (±10°) in the estimate of incidence angle and so is not an important consideration in this example.

The Tibetan Plateau

The Tibetan Plateau is often regarded as an isostatically-compensated block of uplifted crustal rock with an average elevation of 5 km (e.g. Bird and Toksöz, 1977). According to the ultrasonic modeling results, we expect that Rayleigh waves crossing the margins of such a block will be scattered at the

edges of the block and the waveforms distorted. To investigate the effect of the Tibetan Plateau on Rayleigh waves propagating across it we compare real and model-synthetic Rayleigh wave seismograms for the propagation paths shown in Figure 23. The synthetic seismograms are based on model results. The amplitude and phase response of Rayleigh waves incident at the upstep and downstep as the path crosses Tibet are taken from ultrasonic model results.

The Tibetan Plateau is modeled as a constant-elevation feature over a uniform half space. We assume Rayleigh waves follow a great circle path from source to station. We determine the angle the great circle path makes with the edges of the plateau. Then, using the method described in the previous section, model-synthetic Rayleigh wave seismograms are generated by convolving an input waveform with the impulse response of the step model for each of the two edges (up-step and down-step) with the appropriate angles of incidence. Because the Tibetan Plateau is wide compared to a Rayleigh wavelength, interference arising from multiple reflections from opposite edges of the Plateau is neglected. Since there are no WWSSN stations on the northern front of the Plateau, we use the Rayleigh wave recorded at KBL as an input signal to the lens model. The regional attenuation model of Bird (1976) is applied to the synthetic data.

The wavelength scaling implies that the Tibetan Plateau modeled here has an "effective" elevation of 40 km, which is higher by a factor of eight than the true elevation of the plateau. The model assumes crust and mantle are uniform across India and Tibet and the "effective" height of the plateau represents the lumped contribution of crustal thickness differences as well as topography. In spite of this simplification the agreement between real and modeled waveforms is generally good, particularly at longer periods (Figure 24). The observed (WWSSN) seismograms are vertical components of Rayleigh waves from a presumed explosion at Lop Nor (Bird and Toksöz, 1977). Note that the relative

amplitudes between SHL and NDI are similar for both the observed and model-synthetic seismograms. No attempt has been made here to model the small-scale scattering in Tibet and the Himalayas; the short period (<15-20 sec) components of the waveforms therefore do not match as well.

III.5 *CONCLUSIONS*

Using three-dimensional ultrasonic modeling techniques, transmission and reflection coefficients as a function of wavelength and incidence angle are obtained for Rayleigh waves propagating in simple step models. The efficiency of Rayleigh wave transmission and reflection varies strongly with both incidence angle and wavelength. At some incidence angles and frequencies as much as 90% of the incident Rayleigh wave energy is scattered into body waves. Transmission coefficients obtained at normal (90°) incidence agree with those obtained with two dimensional modeling methods and two-dimensional finite-difference methods. An empirical relation between transmission coefficients at different incidence angles is obtained for the case of a vertical step. This relation may be applied to two-dimensional theoretical (numerical) calculations of propagation in more complicated structures to obtain estimates of Rayleigh wave transmission coefficients at oblique incidence angles.

The effect of simple structures on Rayleigh wave propagation in the Earth is demonstrated by convolving the impulse response of the models with real or synthetic dispersed wave trains. Some observed features of Rayleigh waves crossing an ocean-continent margin and the Tibetan Plateau are similar to those predicted from model results. The method may be applied to studies in which surface waves cross regions of strong structural contrast. In Basin-and-Range provinces, for example, where crustal Rayleigh waves traverse numerous steps, strong effects can be expected due to compounding of the effects suffered by passage through a single step.

The ultrasonic model-synthetic method may prove useful in more general problems of three-dimensional surface wave scattering, particularly in situations for which analytic or numerical solutions are difficult to obtain.

REFERENCES

Bird, G.P., 1976. Thermal and Mechanical Evolution of Continental Convergence Zones: Zagros and Himalayas, Ph.D. Thesis, Massachusetts Institute of Technology, Cambridge, Massachusetts.

Bird, P. and M.N. Toksöz, 1977. Strong attenuation of Rayleigh waves in Tibet, *Nature*, *266*, 161-163.

de Bremaecker, J. Cl., 1958. Transmission and reflection of Rayleigh waves by corners, *Geophysics*, *23*, 253-266.

Capon, J., 1970. Analysis of Rayleigh-wave multipath propagation at LASA, *Bull. Seis. Soc. Am.*, *60*, 1701-1731.

Capon, J., 1971. Comparison of Love- and Rayleigh-wave multipath propagation at LASA, *Bull. Seis. Soc. Am.*, *61*, 1327-1344.

Chen, T.C. and L.E. Alsop, 1979. Reflection and transmission of obliquely incident Rayleigh waves at a vertical discontinuity between two welded quarter-spaces, *Bull. Seis. Soc. Am.*, *69*, 1409-1423.

Drake, L.A., 1972. Love and Rayleigh waves in nonhorizontally layered media, *Bull. Seis. Soc. Am.*, *62*, 1241-1258.

Drake, L.A. and B.A. Bolt, 1980. Love waves normally incident at a continental boundary, *Bull. Seis. Soc. Am.*, *70*, 1103-1123.

Dziewonski, A.M., A.L.Hales, and E.R. Lapwood, 1975. Parametrically simple earth models consistent with geophysical data, *Phys. Earth Plan. Int.*, *10*, 12-48.

Evernden, J.F., 1953, Direction of approach of Rayleigh waves and related problems, Part I, *Bull. Seis. Soc. Am.*, *43*, 335-374.

Evernden, J.F., 1954. Direction of approach of Rayleigh waves and related problems, Part II, *Bull. Seis. Soc. Am.*, *44*, 159-184.

Fuyuki, M. and M. Nakano, 1984. Finite difference analysis of Rayleigh wave transmission past an upward step change, *Bull. Seis. Soc. Am.*, *74*, 893-911.

Kato, Y. and A. Takagi, 1956. Model seismology (part 3): wave propagation in the step-shaped structure and on the cliff, *Sci. Rep. Tohoku Univ., ser. 5*, *8*, 74-86.

Knopoff, L. and A. Gangi, 1960. Transmission and reflection of Rayleigh waves by wedges, *Geophysics*, *25*, 1203-1214.

Lewis, D. and J.W. Dally, 1970. Photoelastic analysis of Rayleigh wave propagation in wedges, *Geophysics*, *75*, 3387-3398.

Malichewsky, P., 1976. Surface waves in media having lateral heterogeneities, *Pure and Appl. Geophys.*, *114*, 833-843.

Martel, L., M. Munasinghe, and G.W. Farnell, 1977. Transmission and reflection of Rayleigh waves through a step, *Bull. Seis. Soc. Am.*, *67*, 1277-1290.

Jarr, A. and L.E. Alsop, 1967. Transmission and reflection of Rayleigh waves . vertical boundaries, *J. Geophys. Res.*, *72*, 2169-2180.

Nathman, D.R., 1980. Rayleigh Wave Scattering Across Step Discontinuities, M.S. Thesis, Massassachusetts Institute of Technology, Cambridge, MA.

Pilant, W.L., L. Knopoff and F. Schwab, 1964. Transmission and reflection of surface waves at a corner, 3. Rayleigh waves (experimental), *Jour. Geophys. Res.*, *69*, 291-298.

Toksöz, M.N., 1983. Development of ultrasonic modeling technique for the study of crustal inhomogeneities, Final Report to Air Force Geophysics Laboratory, AFGL-TR-83-0070.

White, J.E., 1965. Seismic Waves: Radiation, Transmission, and Attenuation, New York, McGraw Hill.

FIGURE CAPTIONS

Figure 12. Geometry of the models used in this study. Source transducer is located at point *S*. Reflected or transmitted waves are recorded at points *R* or *T*. Cross sections of two steps used are shown below. The source and receiver transducers are identical. Each transducer is made of a piezoelectric unit embedded in a lucite wedge as shown at the bottom of the figure. This arrangement maximizes the Rayleigh wave response. The wedges are coupled to the model with vacuum grease.

Figure 13. Waveforms of Rayleigh waves transmitted across a 3mm vertical step. The top trace is the input signal, obtained by putting source and receiver 10 cm apart, on the half space. The small pulse arriving 1.0 μsec before the Rayleigh wave is an S wave excited at the step. The vertical scales on the seismograms have been expanded by the scaling factors shown at the start of each trace. *A:* Transmission in the up-step direction. *B:* Transmission in the down-step direction.

Figure 14. Energy transmission coefficients for the Rayleigh waves in Figure 13. The horizontal axis is normalized frequency ($\hat{f} = \frac{h}{\lambda}$), where h is the step height and λ is the wavelength. Curves are shown for three angles of incidence. *A:* Transmission in the up-step direction. *B:* Transmission in the down-step direction.

Figure 15. Waveforms of Rayleigh waves reflected from the 3mm vertical step. Note the secondary reflection corresponding to a reflection from the *upper* edge of the step. *A:* Reflection from the upstep. *B:* Reflection from the

downstep.

Figure 16. Energy reflection coefficients for the reflected Rayleigh waves in Figure 15. Note the change of vertical scale from Figure 14. *A:* Reflection from the upstep. *B:* Reflection from the downstep.

Figure 17. Seismograms of Rayleigh waves transmitted across *(A)* and reflected from *(B)* the 3mm, 60° ramp. Propagation is in the up-step direction The seismograms in *(B)* were high-pass filtered at 0.3 MHz at the time of recording to enhance the signal-to-noise ratio.

Figure 18. Energy transmission and reflection coefficients for the Rayleigh waves in Figure 17. *A:* Upstep transmission. *B:* Upstep reflection. Note the difference in the amplitude scales.

Figure 19. Energy transmission data of Figure 14a after application of the empirical relation of Equation (3). The transmission curves for the different incidence angles now coincide.

Figure 20. The effect of the 3 mm vertical step *(A)* and ramp *(B)* models on a dispersed wave train. The input signal (top trace) is a linear chirped sinusoid, whose frequency increases from 0.2 to 2.0 MHz in 60 μsec. The corresponding range of the ratio of step height/wavelength ($\hat{f}$) is 0.2 to 2.

Figure 21. The region in h-λ space in which the ultrasonic model results from the 3 mm models may be reliably used. Units of h and λ are arbitrary. In the shaded areas repeatability and consistency of a given experiment is not assured. The usable and unusable regions are demarcated by the maximum and

minimum usable normalized frequencies. The box shows the region allowed for modeling Rayleigh waves in the period range 15-40 sec (50-150 km wavelength). Thus step heights in the range 30-100 km may be modeled successfully over this period range.

Figure 22. *A.* WWSSN vertical component recordings of the Rayleigh waves from an earthquake in the Loyalty Islands (9/6/81, $11^{h}02^{m}40.8^{s}$; 21.488° S, 169.600° E, depth=31 km, m_b=5.9, M_s=6.2). The angle at which the great-circle crosses the continental margin is shown next to the continental stations. *B.* Model synthetic seismograms using the 3mm, 60° ramp scaled to 60 km height.

Figure 23. Rayleigh wave paths across the Tibetan Plateau from an explosion at the Lop Nor test site (14 October, 1970). Reproduced from Bird (1976). *Inset:* Three-dimensional model of the Tibetan Plateau used to generate model-synthetic seismograms for the paths Lop Nor-NDI and Lop Nor-SHL.

Figure 24. Comparison of real seismograms (solid lines) with model-synthetic seismograms (dashed lines) using the lens model of Figure 12. All seismograms have been low-pass filtered at 10 second period.

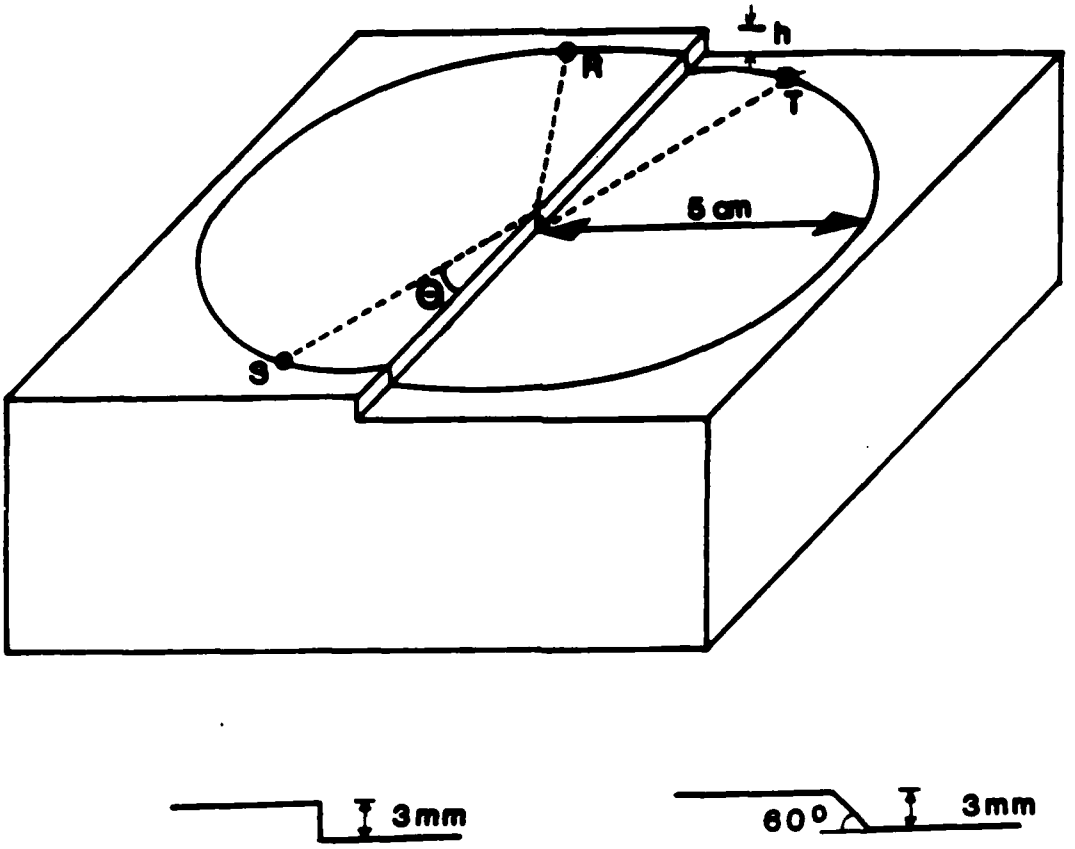

Figure 12.

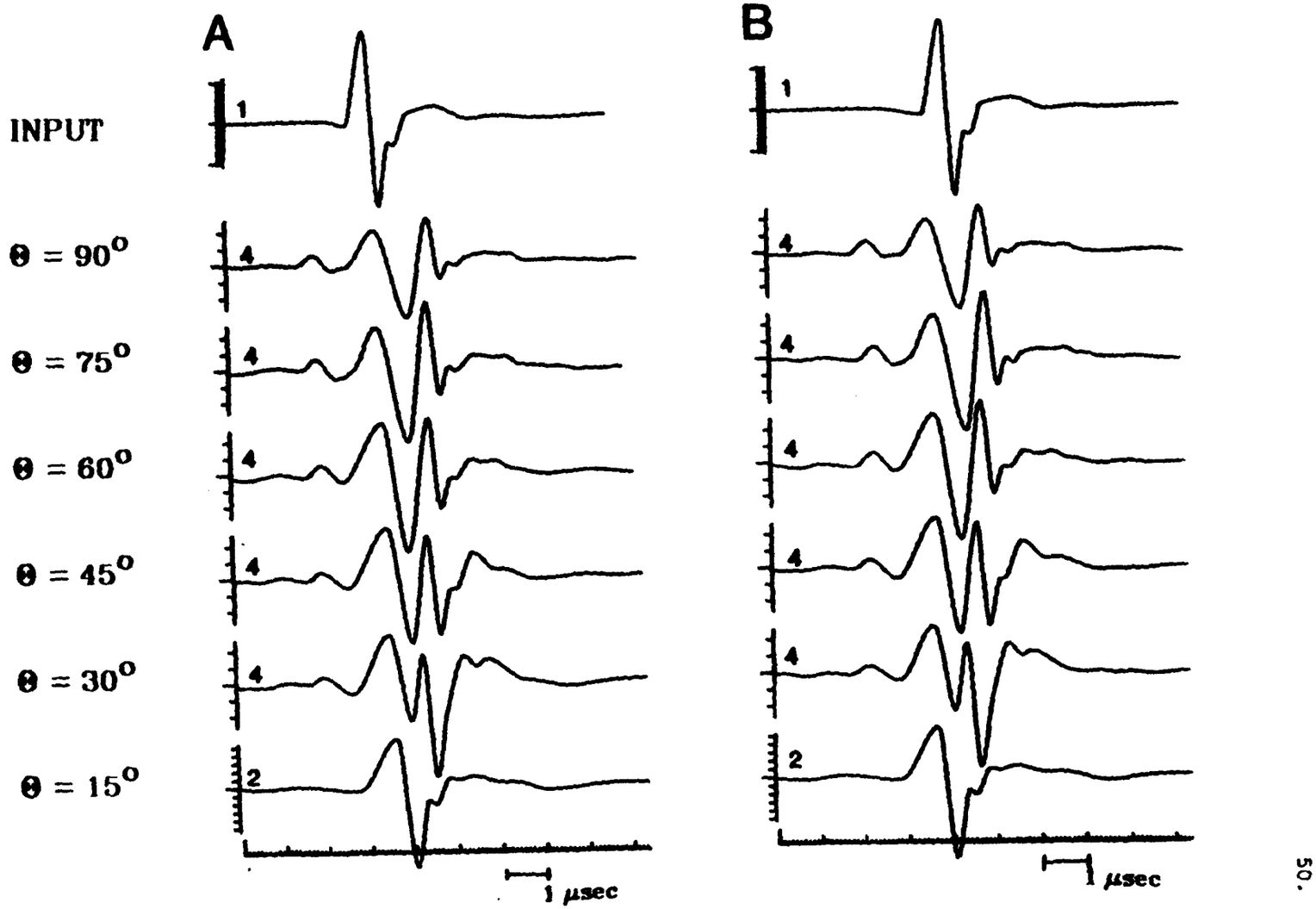

Figure 13.

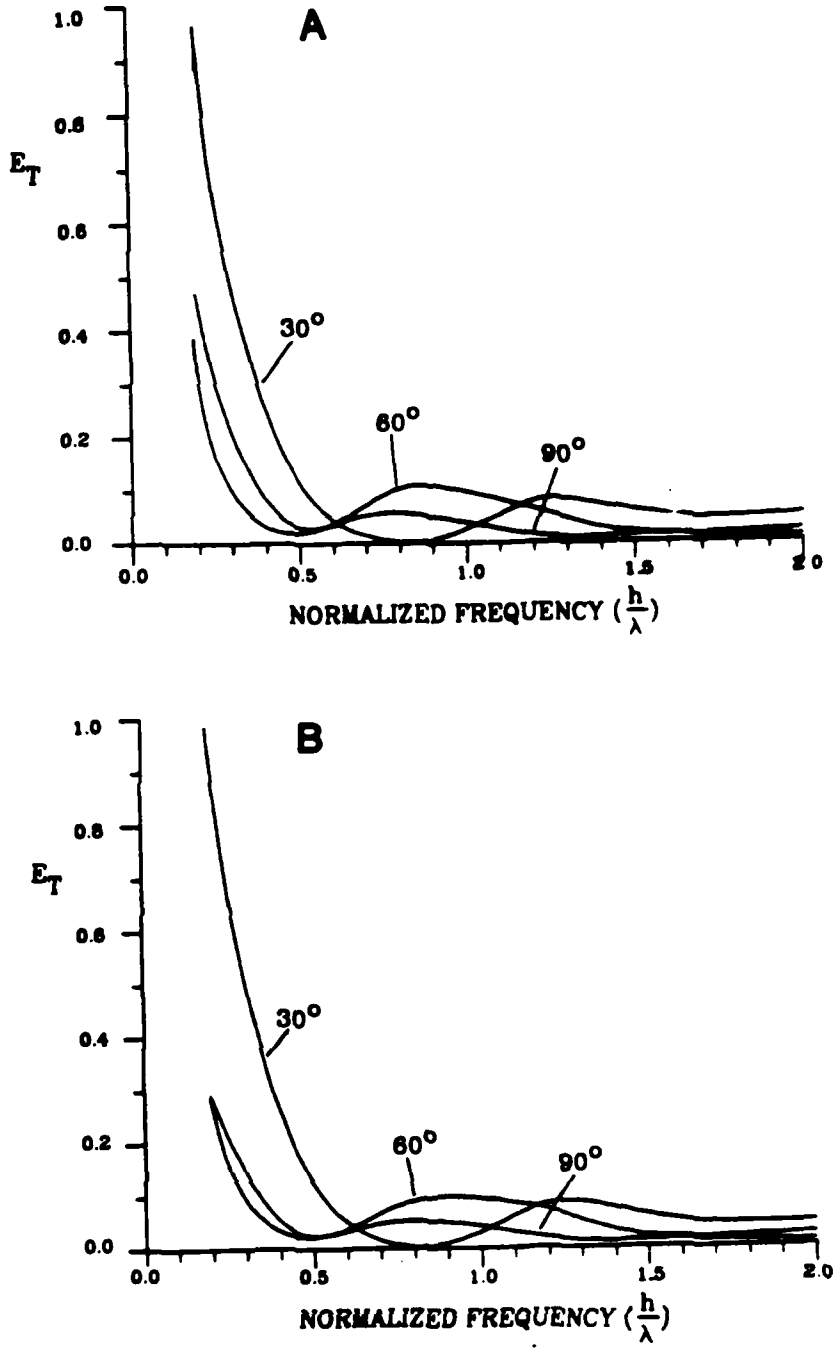
A
B
E_T
1.0
0.8
0.6
0.4
0.2
0.0
30°
60°
90°
0.0
0.5
1.0
1.5
2.0
NORMALIZED FREQUENCY ($\frac{h}{\lambda}$)

Figure 14.

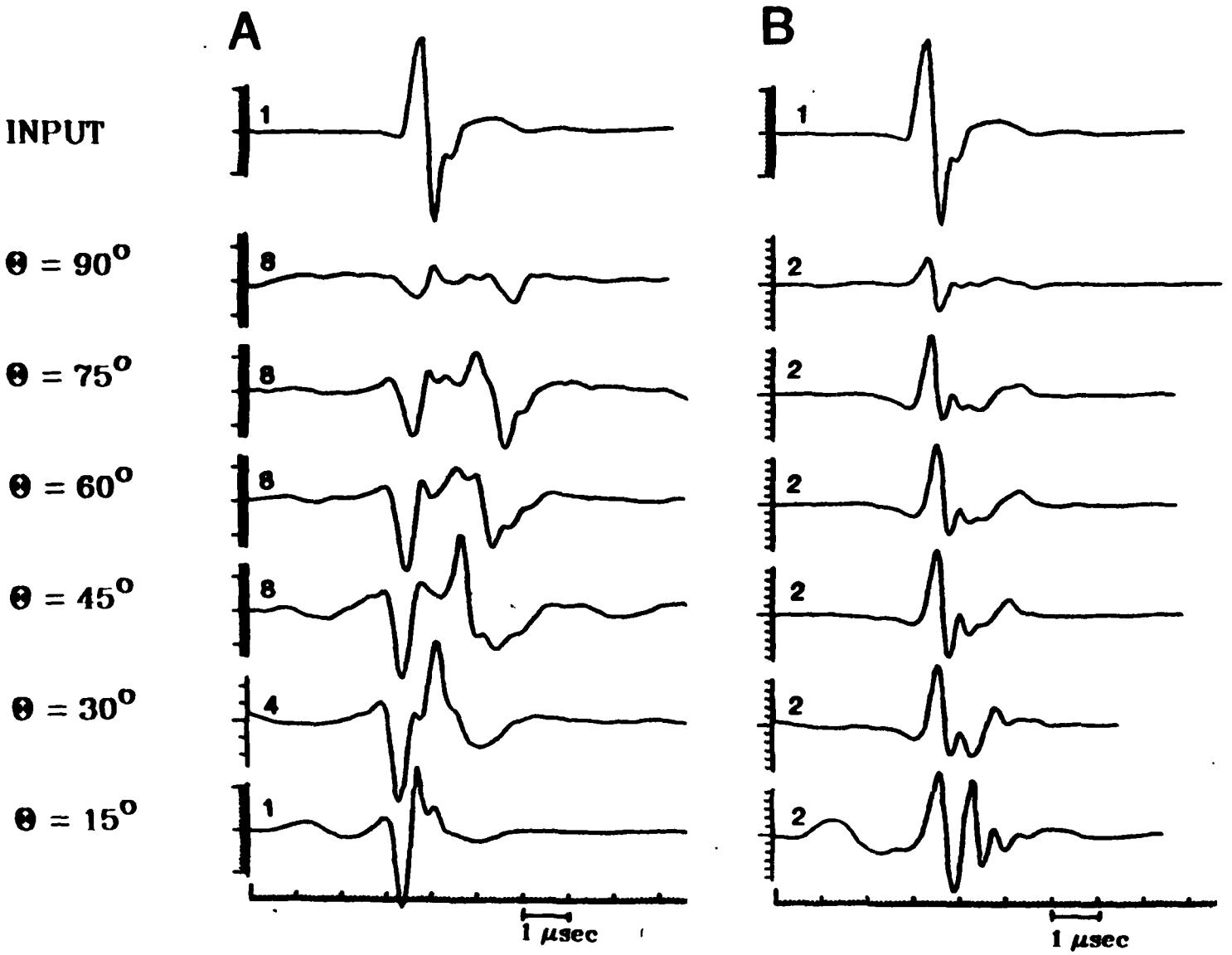

Figure 15.

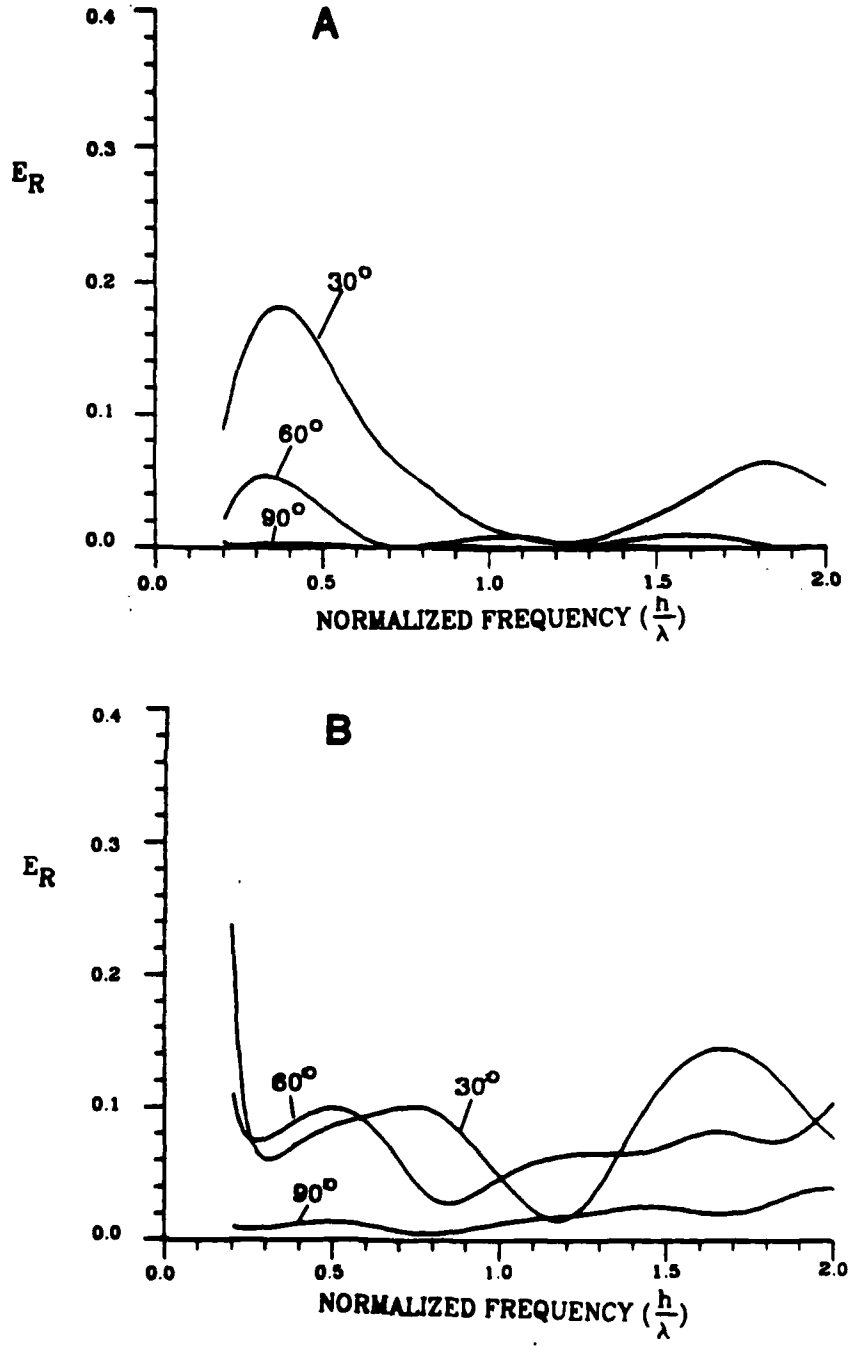
A
E_R
0.4
0.3
0.2
0.1
0.0
30°
60°
90°
0.0
0.5
1.0
1.5
2.0
NORMALIZED FREQUENCY ($\frac{h}{\lambda}$)
B
E_R
0.4
0.3
0.2
0.1
0.0
60°
30°
90°
0.0
0.5
1.0
1.5
2.0
NORMALIZED FREQUENCY ($\frac{h}{\lambda}$)

Figure 16.

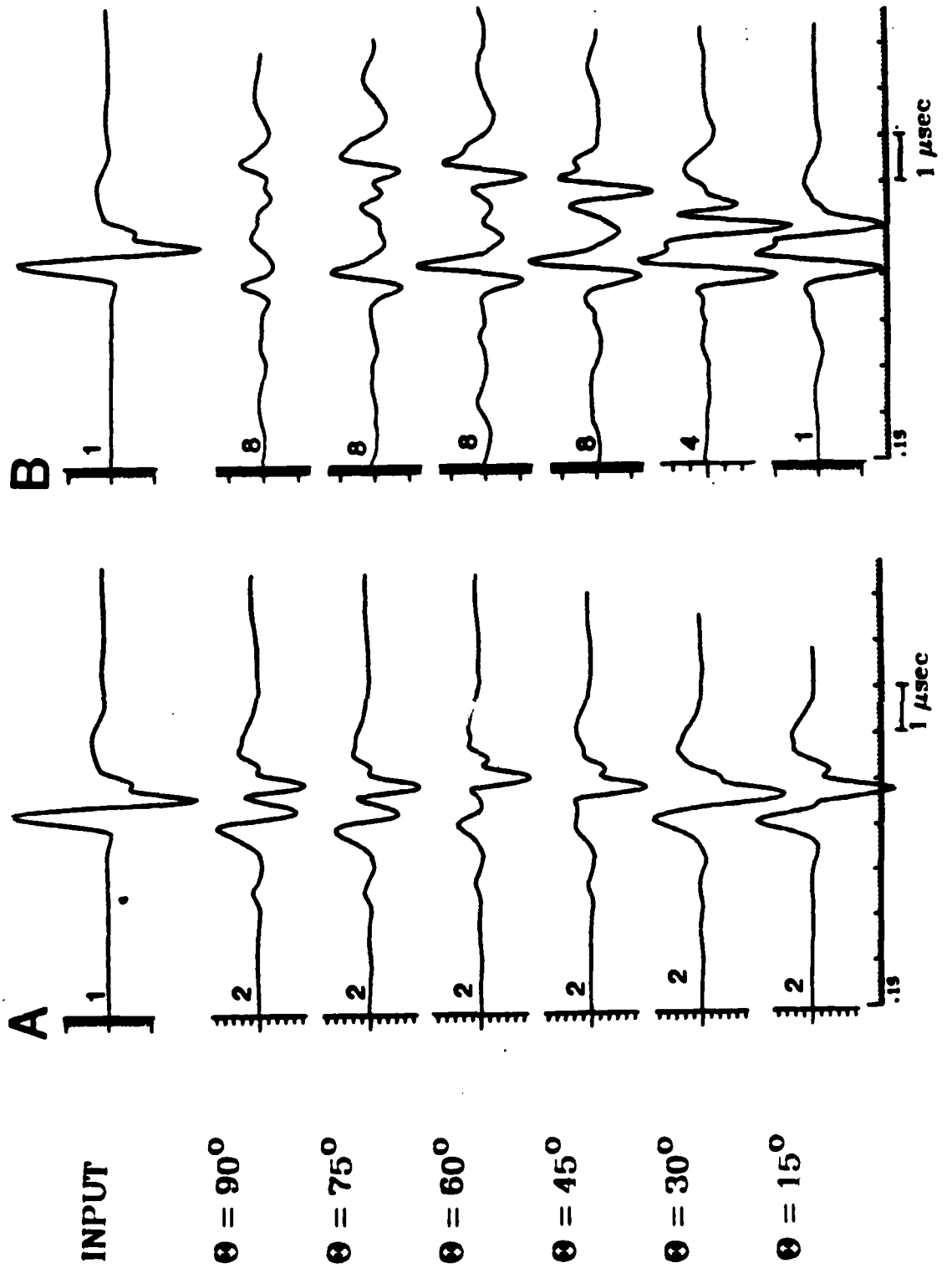

Figure 17.

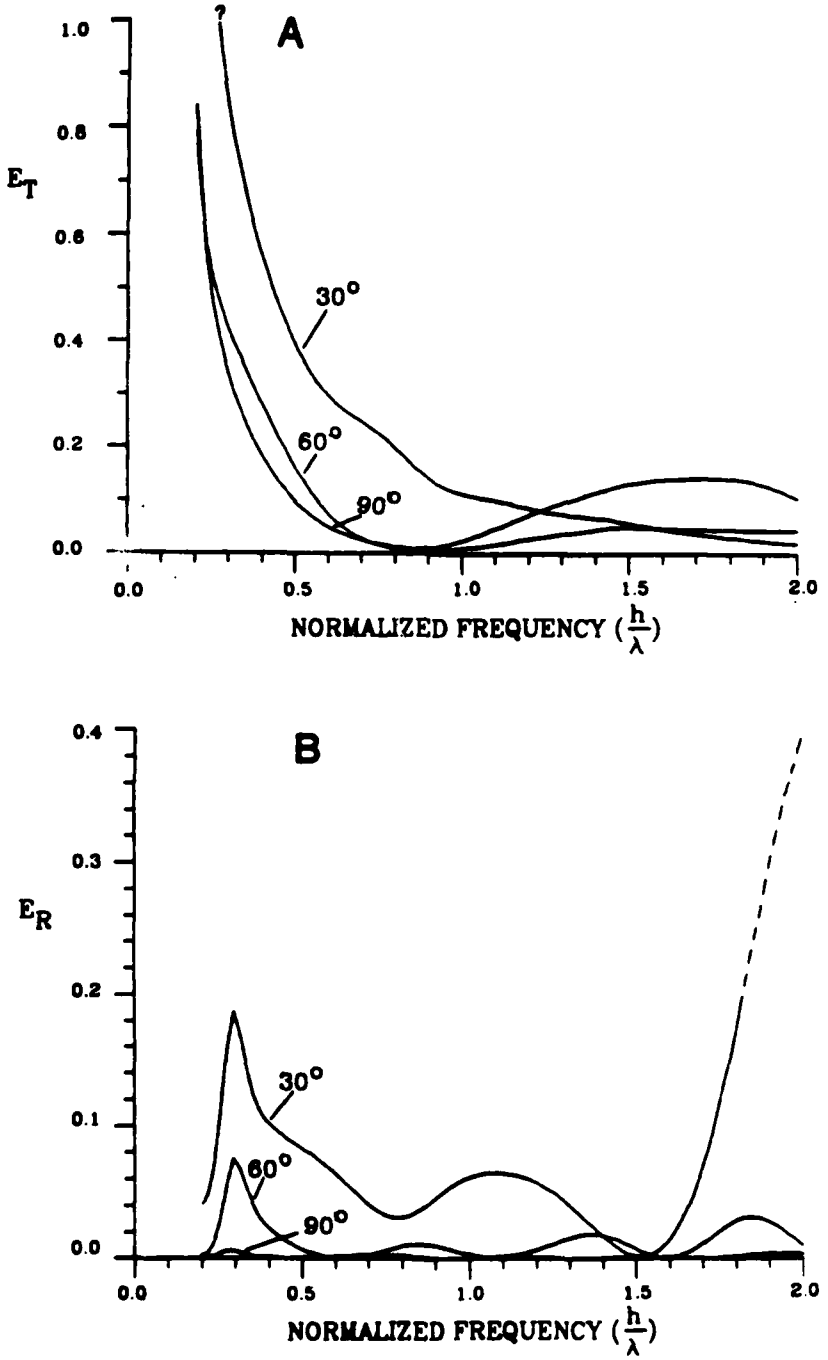
A
1.0
0.8
0.6
0.4
0.2
0.0
E_T
30°
60°
90°
0.0
0.5
1.0
1.5
2.0
NORMALIZED FREQUENCY ($\frac{h}{\lambda}$)
B
0.4
0.3
0.2
0.1
0.0
E_R
30°
60°
90°
0.0
0.5
1.0
1.5
2.0
NORMALIZED FREQUENCY ($\frac{h}{\lambda}$)

Figure 18.

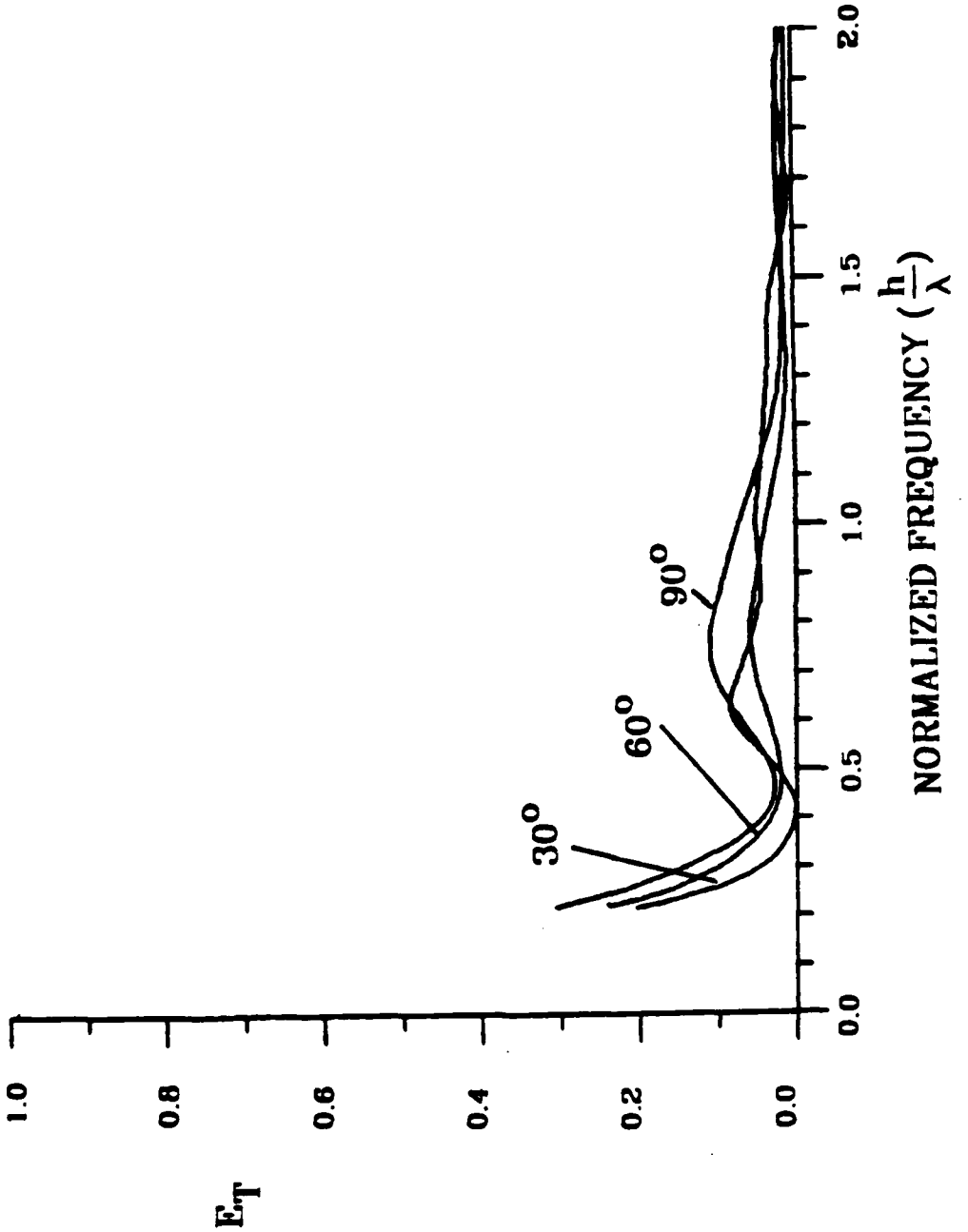
1.0
0.8
0.6
0.4
0.2
0.0
E_T
0.0
0.5
1.0
1.5
2.0
NORMALIZED FREQUENCY ($\frac{h}{\lambda}$)
30°
60°
90°

Figure 19.

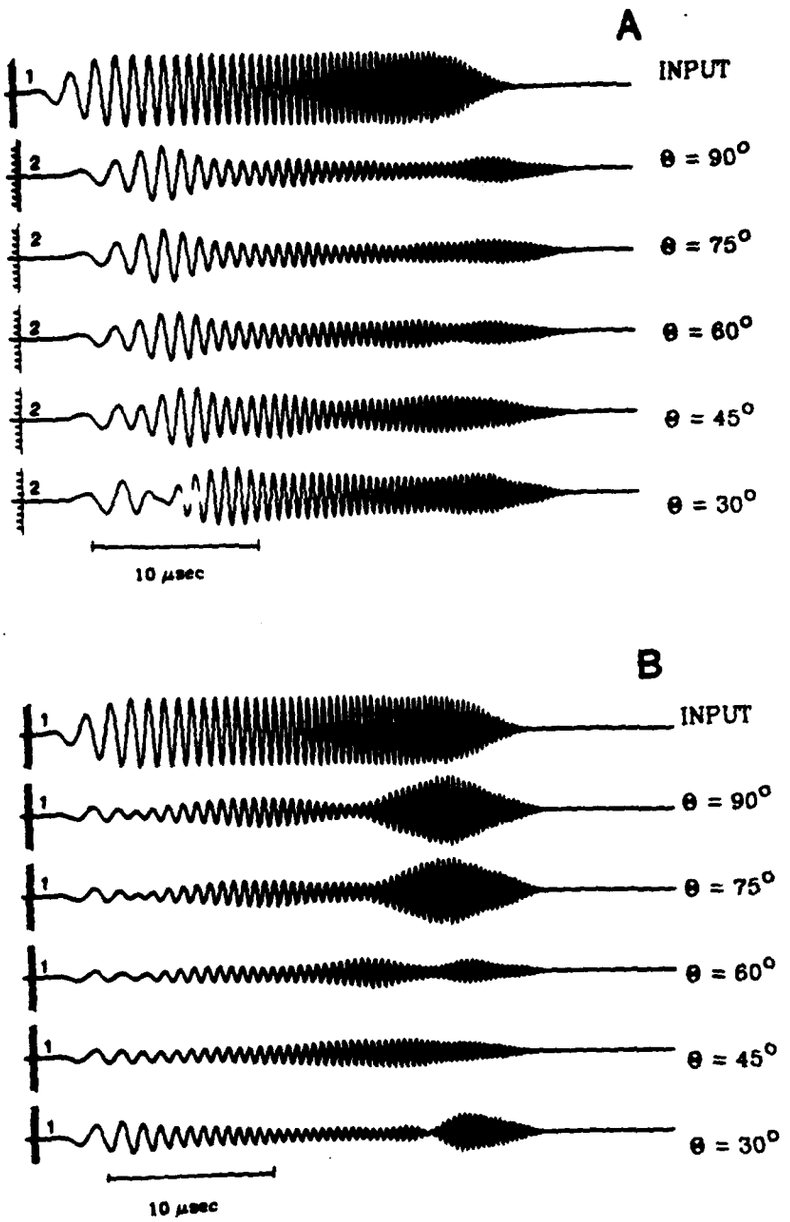
A
INPUT
θ = 90°
θ = 75°
θ = 60°
θ = 45°
θ = 30°
10 μsec
B
INPUT
θ = 90°
θ = 75°
θ = 60°
θ = 45°
θ = 30°
10 μsec

Figure 20.

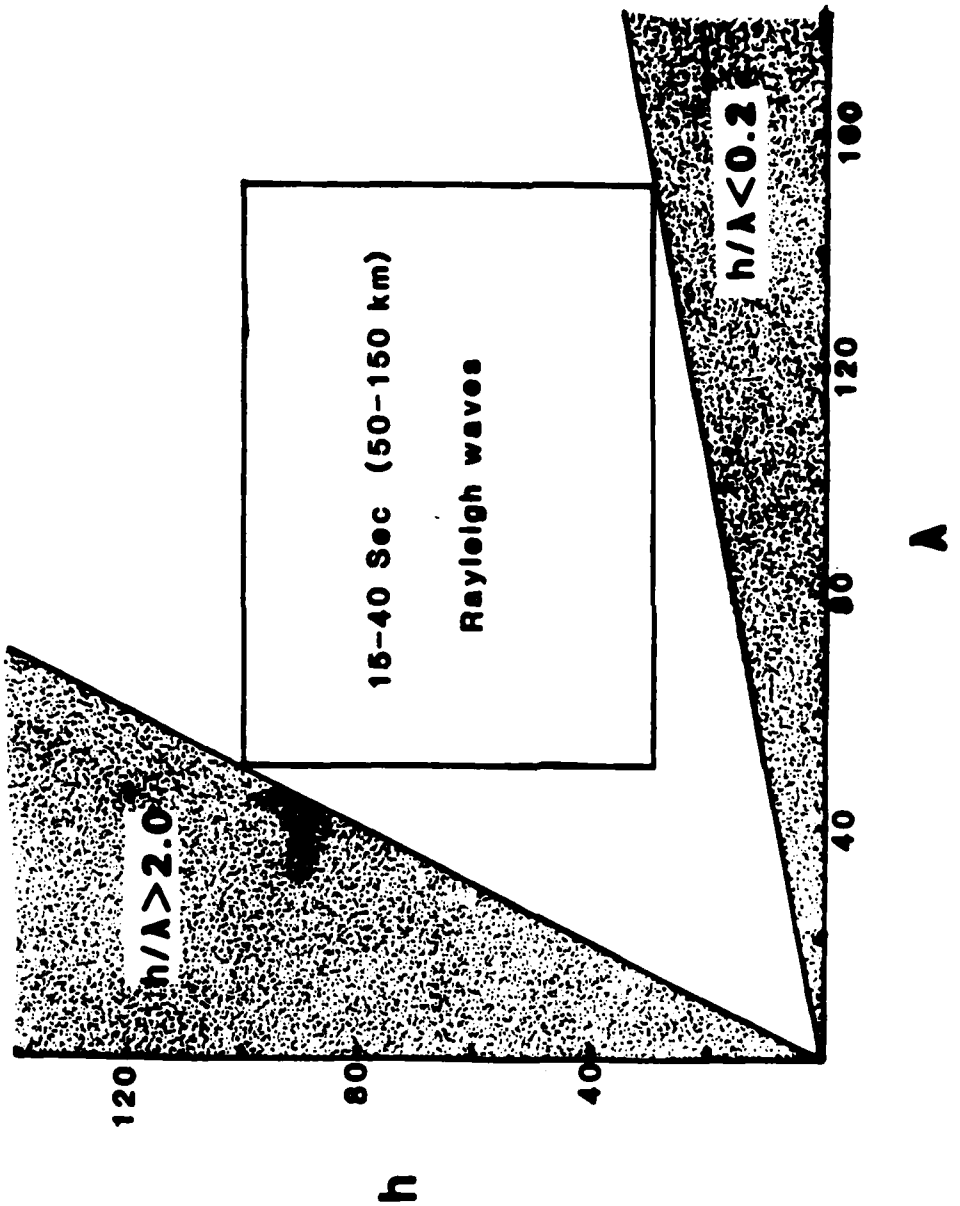
h/λ>2.0
15-40 Sec (50-150 km)
Rayleigh waves
h/λ<0.2
120
80
40
h
40
80
120
100
λ

Figure 21.

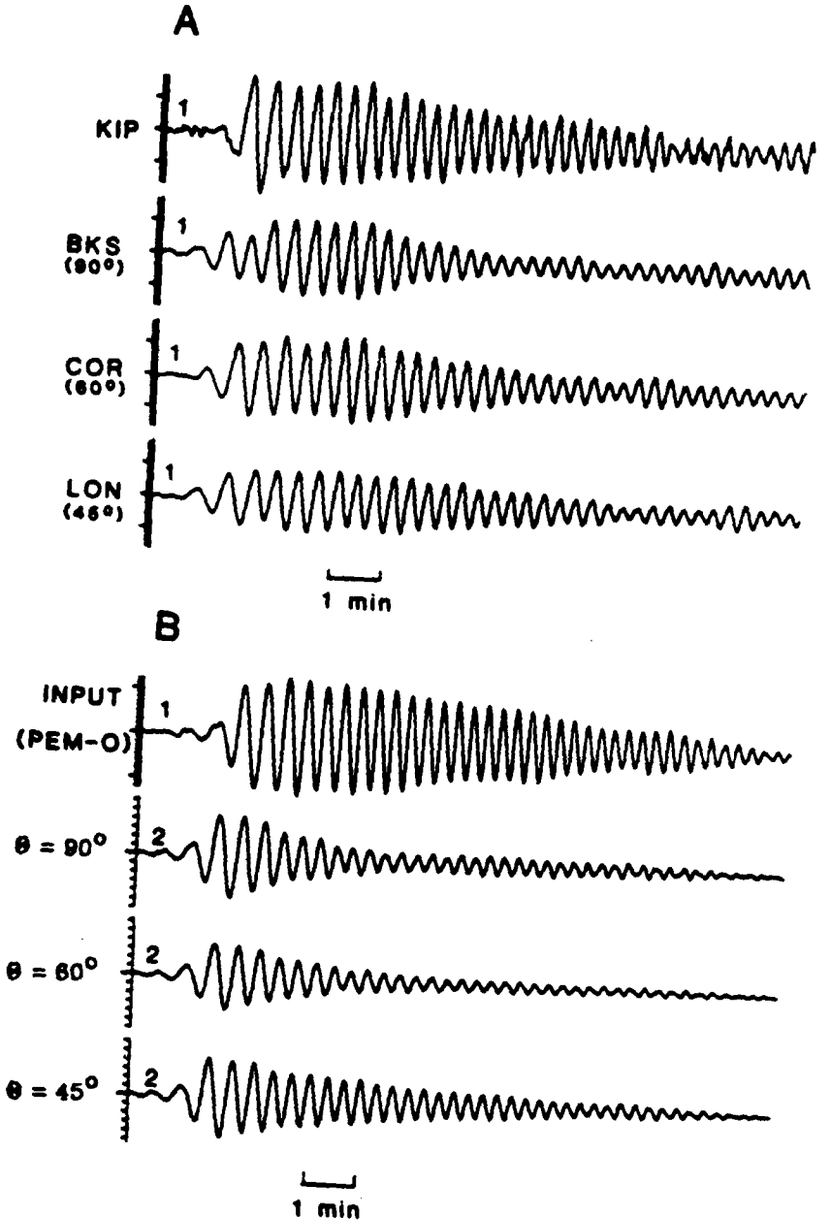
A
KIP
1
BKS
(80°)
1
COR
(60°)
1
LON
(46°)
1
1 min
B
INPUT
(PEM-O)
1
θ = 90°
2
θ = 60°
2
θ = 45°
2
1 min

Figure 22.

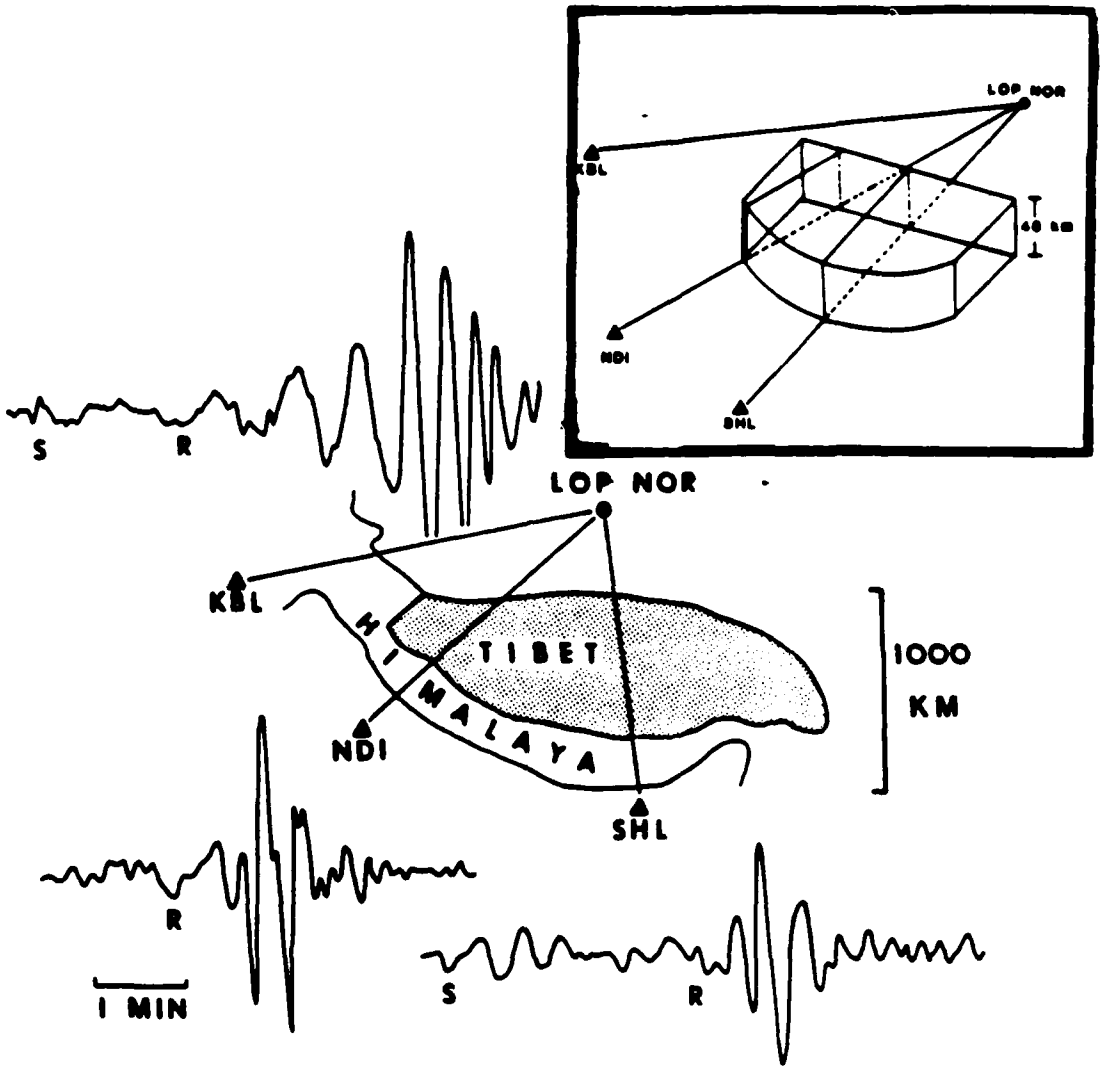

Figure 23.

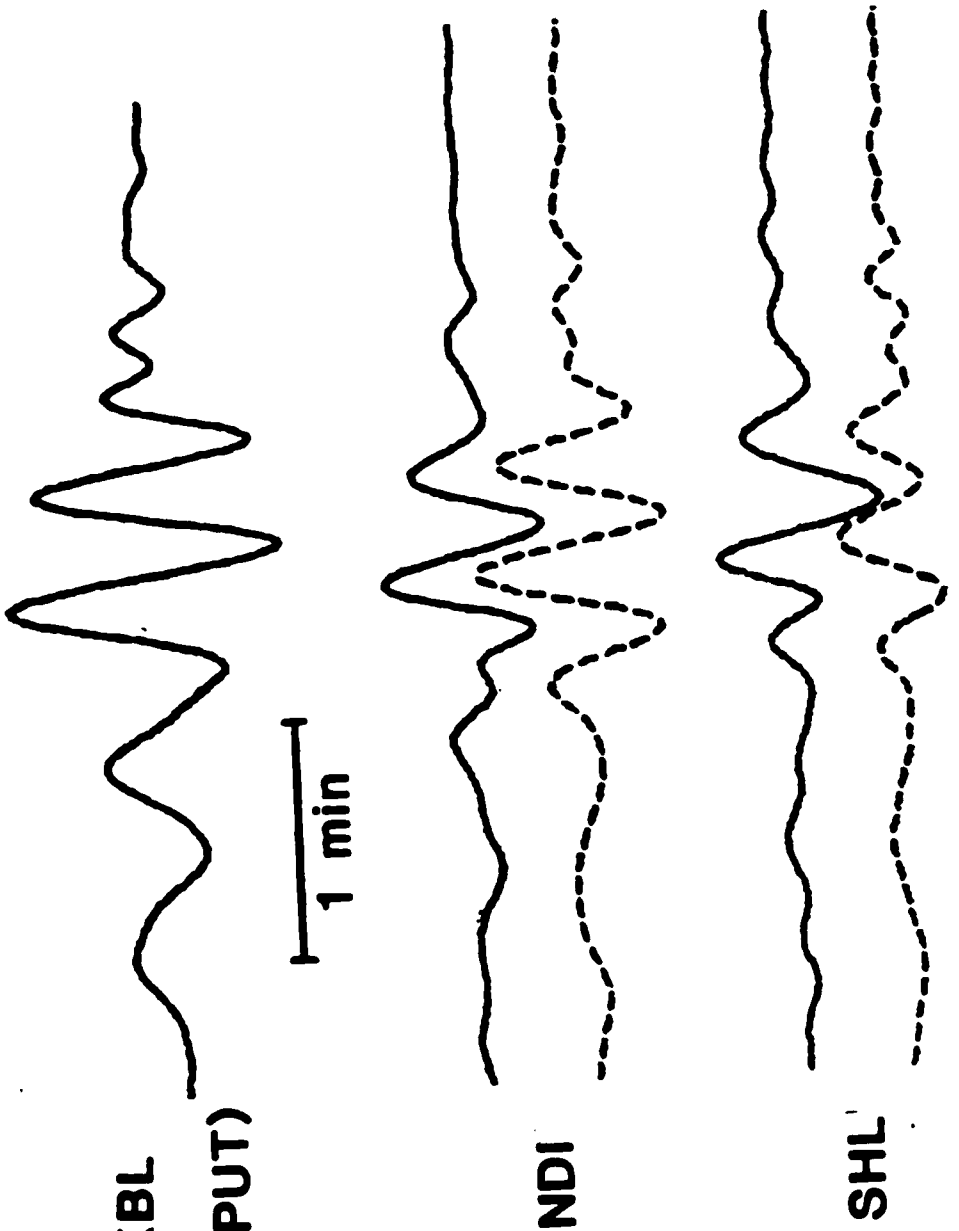

Figure 24.

IV. CONTRACT PUBLICATIONS

Bullitt, J.B. and M.N. Toksöz, 1985. Three dimensional ultrasonic modeling of Rayleigh wave propagation, *Bull. Seism. Soc. Am.*, in press.

Chamuel, J.R., 1984a. Rayleigh wave travsmission reciprocity past a step change in elevation, *J. Acoust. Soc. Am.*, *75*, 1491-1494.

Chamuel, J.R., 1984b. New ultrasonic modeling findings on Rayleigh wave propagation and their implications, J. Acoust. Soc. Am., 75, 1495-1504.

Toksöz, M.N., F. Pardo-Casas, and D. Nathman, 1985. Rayleigh wave scattering by surface discontinuities: Two-dimensional models, in preparation.

V. PARTICIPATING SCIENTIFIC PERSONNEL

M.N. Toksöz
J. Bullitt
J. Chamuel
K. Coyner
T. Keho
R. Nowack
K. Tubman
S. Turcotte
R. Turpening

END

FILMED

1-86

DTIC